R. & M. No. 3447

MINISTRY OF AVIATION

AERONAUTICAL RESEARCH COUNCIL
REPORTS AND MEMORANDA

A Critical Review of Existing Methods of Calculating the Turbulent Boundary Layer

By B. G. J. Thompson, Ph.D.

LONDON: HER MAJESTY'S STATIONERY OFFICE
1967
PRICE £1 4s 0d NET

A Critical Review of Existing Methods of Calculating the Turbulent Boundary Layer

By B. G. J. Thompson, Ph.D.

Communicated by Professor W. A. Mair, University of Cambridge

*Reports and Memoranda No. 3447**
August, 1964

Summary.

Existing methods of calculating the incompressible turbulent boundary layer have been critically examined and the results that they give compared with a large amount of published experimental data. The investigation has shown that different methods of calculating shape-factor development give, in general, widely different results and are in some cases very inaccurate. Head's entrainment equation proved generally the most satisfactory.

It was also found that the measured growth of momentum thickness usually disagreed with the predictions of the two-dimensional momentum integral equation, even far from separation, indicating the presence of substantial three-dimensional effects. However, no overall improvement in agreement with experiment could be obtained by using the quadrature formulae proposed by various authors.

LIST OF CONTENTS

Section

1. Introductory
   - 1.1 Introduction
   - 1.2 The basic equations of the turbulent boundary layer
   - 1.3 The necessity for approximate methods of solution
   - 1.4 Approximate similarity solutions
   - 1.5 Approximate solutions using the integral relationships
   - 1.6 The application of calculation methods
   - 1.7 Discussion
2. Published Experimental Information on Turbulent Boundary Layer Development
3. Methods of Calculating Momentum Thickness Development
   - 3.1 Calculations performed
   - 3.2 The results of the calculations
   - 3.3 Discussion of the results of the step-by-step calculations using the simple momentum equation
   - 3.4 Discussion of the results obtained by using alternative forms of the momentum integral equation
   - 3.5 Conclusions

* Replaces A.R.C. 26 109.

LIST OF CONTENTS—*continued*

Section

4. Methods of Calculating Shape-Factor Development
- 4.1 The basis for comparisons of shape-factor calculations
- 4.2 The generalised auxiliary equation
- 4.3 The shape-factor calculations
- 4.4 Discussion of results
- 4.5 A review of existing auxiliary equations and further discussion of the comparisons with experiment
  - 4.5.1 Early empirical equations (1930 to 1943)
  - 4.5.2 Later empirical equations of von Doenhoff and Tetervin, Garner and Maskell
  - 4.5.3 The equations of Spence and Norbury
  - 4.5.4 The use of energy equation—the methods of Rotta, Truckenbrodt, Rubert and Persh, Schuh, Tani, Kawasaki, and Walz
  - 4.5.5 The entrainment equation
- 4.6 Stability of shape-factor calculations

5. Conclusions

Notation

References

Appendix—The method of integration of velocity profiles to find θ and δ^*

Illustrations—Figs. 1 to 37

Detachable Abstract Cards

---

1. *Introductory*

1.1. *Introduction*

This examination of existing work differs substantially from previous treatments in giving a large number of direct comparisons between the predictions of the various methods and a wide range of experimental data.

It is found that existing methods often give rise to very different predictions, especially for the development of shape-factor, and furthermore, that, with the exception of the entrainment equation of Head[25], no shape-factor equation provides satisfactory agreement with more than one half of the measured developments that have been used as a basis for the present comparisons. This contrasts with the general impression given by earlier reviews. For example, Duncan, Thom and Young[15], in referring to the auxiliary equations of Spence[60, 61] and Maskell[35] and others, state (on p. 347) that

> 'As far as the accuracy of the final formulae is concerned there is little to choose between them and the choice must therefore largely turn on relative simplicity and convenience for computation. From this point of view, Spence's formula is perhaps the best.'

It appears that the better known methods have been accepted on the basis of the comparatively good results achieved in the very small number of direct comparisons with experiment that have been presented by the original authors. Spence's method, as mentioned above, has been given some prominence although only two published comparisons were shown in the original papers. Similarly, Schlichting[51] describes the method of Truckenbrodt[71] as being

'. . . . reasonably well-founded . . . .',

although in this case only one comparison with experiment was considered.

Such remarks do not reveal the difficulties associated with the calculation of shape-factor and it seems that they reflect the fairly widely held opinion that, except perhaps near to separation, the existing methods give similar results which are never grossly in error and may be considered to be quite satisfactory for practical purposes. Stratford[63], for example, stated (on p. 13) that

'The accuracy of Maskell's predictions is probably highly satisfactory for most pressure distributions, . . .'.

The present results, shown in Figs. 14 to 24, can scarcely be said to support any of the above statements, and lead to the conclusion that the existing situation as regards shape-factor calculation is very unsatisfactory. This had in fact been suggested previously by Clauser[6] and by Ross[44], although their remarks do not appear to have been widely appreciated.

The calculation of the development of momentum thickness is usually less seriously in error when using the forms of the momentum integral equation adopted by the different authors, but, even in this case, appreciable systematic discrepancies can occur, as shown in Figs. 1 to 10, and once again lead to conclusions which contrast with the current opinion as voiced by Thwaites[67], for example, who says (on p. 81), referring to the momentum equations of Truckenbrodt, Maskell, Schuh[55], and Spence,

'Experience suggests that any of . . . . will give values accurate to within about 5 per cent even up to the separation point.'

A few of the existing methods of calculation have been used by different investigators as the basis for design predictions in various circumstances (for example, Schlichting[50] considers the effects of boundary layer growth and separation on the performance of cascades, using Truckenbrodt's method of boundary-layer calculation), and some methods have been extended for use in different physical conditions (for example, Pechau[41] investigates suction distributions on aerofoils, using an extension of Truckenbrodt's method, whilst Cooke[10] adopts the auxiliary equation of Spence for use in the calculation of three-dimensional turbulent boundary layers).

Now, whilst such applications cannot be criticised in themselves as they are the final aims of any attempt to produce a practical method of calculation, the reliability of the various methods does not appear to have been properly assessed beforehand. It is therefore hoped that the contents of this report will go some way towards clarifying the present position.

The existing proposals for the calculation of shape-factor and momentum thickness are separately examined and also the assumptions for profile shape and skin friction that are involved. Attention is given to the problems that arise from the apparently three-dimensional nature of the majority of the measured turbulent layers, as may be inferred from the lack of agreement between the measured momentum growth and the predictions of the two-dimensional momentum integral equation even when far from separation. First, however, the basic equations and variables of the turbulent boundary-layer problem are set out, and the necessity for approximate methods of solution, their structure and main applications, are briefly discussed.

1.2. *The Basic Equations of the Turbulent Boundary Layer*

As described fully in the literature (Schlichting[51], Hinze[28], etc.) the Navier-Stokes equations for incompressible, viscous flow can be time-averaged for a turbulent flow which is steady in the mean. The time-averaged equations can then be simplified by applying order-of-magnitude arguments on the basis of the boundary-layer hypothesis of Prandtl. The time-mean flow is assumed to be two-dimensional and no difficulty is thought to exist concerning the degree of approximation required, except near to separation where higher order terms may be needed (Newman[37], Hewson[27], Ross[44]).

The boundary-layer equations, written in terms of the usual rectangular Cartesian co-ordinates become, with the order of each term written beneath

$$u\frac{\partial u}{\partial x}+v\frac{\partial u}{\partial y}=U_1\frac{dU_1}{dx}+\frac{1}{\rho}\frac{\partial \tau}{\partial y}-\frac{\partial(\overline{u'^2}-\overline{v'^2})}{\partial x} \tag{1}$$

$$\left[\frac{U_1^2}{L_1}\right]\left[\frac{U_1U_2}{L_2}\right]\qquad\qquad\left[\frac{\tilde{u}^2}{L_2}\right]\qquad\left[\frac{\tilde{u}^2}{L_1}\right]$$

$$\frac{\partial \overline{v'^2}}{\partial y}=-\frac{1}{\rho}\frac{\partial p}{\partial y} \tag{2}$$

$$\left[\frac{\tilde{u}^2}{L_2}\right]$$

In equation (1) the shear stress τ is given by

$$\tau=-\rho\,\overline{u'v'}+\mu\frac{\partial u}{\partial y}, \tag{3}$$

U_1, U_2 are the velocity scales in the x and y directions, L_1, L_2 are the corresponding length scales and the scale of the turbulence velocities is represented by u. It is usually assumed that

$$\frac{L_2}{L_1}\approx\frac{U_2}{U_1}\approx\frac{\tilde{u}^2}{U_1^2}\ll 1.$$

Thus the turbulent normal stress term is of a lower order than the remainder and can usually be ignored.

The continuity equation for the mean flow,

$$\frac{\partial u}{\partial x}+\frac{\partial v}{\partial y}=0, \tag{4}$$

also applies.

1.3. *The Necessity for Approximate Methods of Solution.*

For laminar flow, the existence of a known relationship between the shear stress and the velocity gradient completes the set of partial differential equations and exact solution of the boundary-layer equations is mathematically possible. Analytic solutions have been obtained for some simple boundary conditions, similarity solutions being especially important. The numerical solution of any general problem has always been possible in principle, but has only become practicable with the advent of high-speed automatic computers. Relatively simple methods of calculation, sufficiently accurate for engineering applications, have therefore been developed which satisfy the equations of motion only on the average, by making use of integrated forms satisfying suitable local boundary conditions.

An infinity of such integral forms is entirely equivalent to solving the differential equations of motion. In practice, only a very small number of such relationships is needed to describe the boundary-layer development quite adequately, and simple approximate methods would not otherwise be possible.*

In the case of turbulent flows, no universal expression is known relating the Reynolds stresses to the mean velocity distribution, and no exact solutions of the boundary-layer equations are possible.

The problem can be dealt with in two ways, either of which requires an essentially empirical assumption for the missing relationship. We shall consider in turn

(*a*) a restricted range of flows where conditions are such that approximate similarity solutions of the differential equations may be obtained, and

(*b*) methods of solution based upon the integral relationships.

1.4. *Approximate Similarity Solutions.*

Exact similarity solutions are possible for a wide range of external pressure distributions in the laminar case as the whole velocity distribution can be represented by one choice of length and velocity scales. This is not possible for the turbulent layer on a smooth surface, except in two very special cases:

(1) Favourable pressure-gradient flow in a converging wedge (Townsend[68]).

(2) Adverse pressure-gradient flow with zero wall stress (Stratford[63, 64], Townsend[69]).

The turbulent layer may be assumed to be composed of two regions, an inner one depending solely upon local conditions, and an outer one dependent upon the upstream history of the flow, which is mainly responsible for the local overall velocity profile.

Using the assumption of a constant eddy viscosity in the outer region, the choice of a power-law free-stream velocity distribution allows of a similarity solution for this part of the layer, the partial differential equation (1) being reduced to an ordinary differential equation of the Falkner-Skan type. However, the inner region provides the boundary conditions for this solution and strict similarity must be relaxed if matching of the two different regions is to be possible. This leads to a solution in the form of predictions for nearly similar (generally termed 'equilibrium' or 'self-preserving') boundary layers.

Thorough descriptions of this type of solution have been given by Rotta[45] and Townsend[68, 69, 70], the last paper containing a particularly complete discussion with the inclusion of an improved inner region solution suitable for large adverse pressure gradients.

In view of the necessarily completely specified history of the flow, this approach is not useful in the general case of a developing layer and will not be considered further in this account. However, the experimental flows of this type as measured by Clauser[6] are of interest, as will be seen later.

---

* It will be recognised that only one or two integral parameters are needed to define quite closely any well behaved, continuous curve whose end conditions are also partly specified. For example, the velocity distributions in the boundary layer can be specified by one or two ratios of the integral moments of that distribution taken about the y-axis. Similarly, probability distributions are defined by skewness and flattening factors as well as their mean values and end conditions.

1.5. *Approximate Solutions using the Integral Relationships.*

The boundary-layer equation (1) may be integrated, after eliminating v by means of the continuity equation (4), and multiplication by $u^m y^n$. A doubly infinite family of ordinary differential equations is obtained and has been considered by Tetervin and Lin[66], Truckenbrodt[71] and Walz[72], but apart from an attempt to use the moment-of-momentum equation by Granville[22] only the first two members of this family have been used in calculations.

These are important because of their physical significance and can be derived in an alternative manner by considering the flux, through a control volume, of momentum and kinetic energy respectively. They are the momentum integral equation ($m = 0$, $n = 0$),

$$\frac{d\theta}{dx} = \frac{c_f}{2} - (H+2)\frac{\theta}{U_1}\frac{dU_1}{dx} + \left[\frac{1}{U_1^2}\frac{d}{dx}\int_0^\infty (\overline{u'^2} - \overline{v'^2})\, dy\right], \tag{5}$$

and the energy integral equation ($m = 1$, $n = 0$),

$$\frac{1}{2}\frac{d}{dx}(U_1^3 \epsilon) = \int_0^\infty \frac{\tau}{\rho}\frac{\partial u}{\partial y}\, dy + \left[\int_0^\infty u \frac{\partial}{\partial x}(\overline{u'^2} - \overline{v'^2})\, dy\right]. \tag{6}$$

The integral variables,

$$H = \frac{\delta^*}{\theta} \qquad \text{where} \qquad \delta^* = \int_0^\infty \left(1 - \frac{u}{U_1}\right) dy,$$

$$\theta = \int_0^\infty \frac{u}{U_1}\left(1 - \frac{u}{U_1}\right) dy,$$

and

$$H_\epsilon = \frac{\epsilon}{\theta} \qquad \text{where} \qquad \epsilon = \int_0^\infty \frac{u}{U_1}\left[1 - \left(\frac{u}{U_1}\right)^2\right] dy,$$

appear quite naturally in these equations, and it is for this reason that they are used in the majority of analyses. Some authors, thinking particularly in terms of similarity solutions have disparaged the use of these parameters (*see*, for example, Ross[44], Rotta[46], and Kawasaki[29]).

It is usually supposed that the distribution of mean velocity through the layer can be adequately represented by one local shape parameter and one length scale. Two ordinary differential equations are then used to calculate the distributions of these dependent variables along the surface.

The momentum integral equation (5) is almost always employed to calculate the length scale, which then naturally becomes θ. In terms of the scale Reynolds' number (R_θ), it becomes

$$\frac{dR_\theta}{dx} = \frac{U_1}{\nu}\frac{c_f}{2} - (H+1)\frac{R_\theta}{U_1}\frac{dU_1}{dx} + \left[\begin{matrix}\text{smaller order} \\ \text{terms.}\end{matrix}\right] \tag{7}$$

The shape-factor or form-parameter equation (also called the auxiliary equation) is used to calculate the development of $H(x)$, or some related parameter, and is of the form,

$$\theta\frac{dH}{dx} = F\left(H, R_\theta, \frac{\theta}{U_1}\frac{dU_1}{dx}\right). \tag{8}$$

Any one of the other integral equations may be introduced to give the form of this equation if the integrals involving the distribution of the turbulence shear stress can be represented in terms of the local properties of the velocity distribution. In the momentum equation, the turbulent shear stress appears only in as far as it influences the local skin-friction coefficient, c_f. Fortunately this can be related to the local velocity profile quite accurately, by means of a relationship of the form

$$f(c_f, R_\theta, H) = 0. \tag{9}$$

However, the other expressions require knowledge of the whole turbulent stress distribution which will depend upon the upstream history of the layer, as the stresses are related more to the local flow accelerations than to the local velocities. A fundamental uncertainty thus exists, even in two-dimensional flow when the simple boundary-layer approximations are valid, because the existing forms of (8), whether derived from the integral equations or obtained empirically, are unlikely to allow properly for the upstream influence on the local stress-velocity relationship. The equilibrium boundary layer has, however, a well defined history which can be expressed in terms of local quantities, and this simplification is the main attraction for the investigation of such flows.

The description of the mean velocity distribution requires the adoption of a velocity profile family. This can be done explicitly, profile shapes being defined most generally by

$$\frac{u}{U_1} = f\left(H, R_\theta, \frac{y}{\theta}\right). \tag{10}$$

Alternatively the family may be implied by any relationship between shape factors such as H and H_e, or H and $H_{\delta-\delta^*}$.

1.6. *The Application of Calculation Methods*

For solid-wall layers we have in effect a set of equations (7), (8) and (9) from which the distributions of any three of the variables U_1, R_θ, H, c_f may be calculated if the initial conditions and the distribution of the fourth variable are given.

Normally, $U_1(x)$ is supplied from a potential-flow solution or by experiment, and calculated values of H or c_f can be used to indicate the proximity of the layer to separation. The drag of aerofoils in unseparated flow can be obtained from calculations of $\theta(x)$ (Squire and Young[62]). The displacement thickness $\delta^*(x)$ can be calculated to allow corrections to the external velocity distribution for diffusers and aerofoils and Preston[43] and Spence[59] provide methods of correcting lift and drag for aerofoils in this way.

The calculation of $\theta(x)$ and $H(x)$ for given $U_1(x)$ is the orthodox problem and forms the main task of any calculation method and it has been used exclusively in this report to test proposed methods by comparing their predictions with experiment.

The so-called 'inverse problem' involves calculation with a different choice of dependent variables. Bradshaw[4] and earlier, von Doenhoff and Tetervin[13], have briefly considered the most important case where $H(x)$ is given and $U_1(x)$ is to be predicted. Stratford[63], and Fernholz[18] have used this technique to design 'optimum' diffusers, whilst Wortmann[74] (1955) has calculated improved low-drag aerofoils on a similar basis.

1.7. *Discussion.*

In order to establish the accuracy of any method of calculation we should ideally examine the accuracy of the individual assumptions by making direct comparisons with as wide a range of experimental measurements as possible and consider the results of these comparisons along with the way in which the assumptions have been used in deriving the final equations. In fact, the major problem is that of predicting the shape-factor variation and it will be shown later that this is most profitably done on the basis of experimental R_θ. The velocity profiles and skin-friction assumptions will also be considered. It is believed that this is a more profitable procedure than discussing the complete method of calculation given by any particular author, as the effects of individual assumptions may well be lost if only the overall results are considered.

2. *Published Experimental Information on Turbulent Boundary-Layer Development.*

In this section we outline the main features of those boundary-layer measurements which have been used later for the comparisons of H and R_θ development. Detailed reviews of the earlier experiments have been made by Ross[44], and Coles[8], but some more recent data have been included in this investigation.

The nominally two-dimensional layers may be conveniently grouped as follows:

2.1. *Equilibrium Layers on Flat Surfaces.*

2.1.1. *Zero pressure gradient* (Klebanoff[31], Hama[24], Dutton[16], Smith and Walker[57], Klebanoff and Diehl[32]).

The experiments of Smith and Walker show the largest number of measurements, especially at high Reynolds numbers. Their results spread appreciably between different experimental runs and some evidence is found of a systematic variation of the inner-law coefficients (A, B) with Reynolds number, on the basis of direct measurements of skin friction.

Their very detailed velocity profile measurements are conveniently tabulated and selected examples have been used in this investigation, after the H and R_θ values had been recalculated. The original values and the results of the recalculations are compared in Fig. 14, where it can also be seen that the experimental momentum growth is in very good agreement with the calculated result for two-dimensional conditions obtained by Coles[7].

The behaviour of the artificially thickened layer measured by Klebanoff and Diehl[32] is of some importance in the present investigation, as the intemittency measurements of Klebanoff[31] were made in this layer at $R_\theta = 7400$, where, as seen in Fig. 14, recovery from the upstream disturbances appears to be complete. This conclusion is supported in a recent, very comprehensive review of the experimental knowledge of the constant pressure boundary layer made by Coles[9], to which reference should be made for further details of this type of flow.

A rather surprising variation between the results obtained by different experimenters in what, at first sight, may be regarded as a comparatively simple turbulent layer, is shown in Fig. 14, where the data of Hama, Dutton, and Ludwieg and Tillmann have been included although they were not used in any of the new calculations. It is important to notice, in this connection, that the values of H and R_θ shown, have not been recalculated by one operator using a single method of integration and a consistent choice of mean line through the scattered velocity measurements that make up each velocity profile. It is the experience of the present author that different operators may obtain consistently quite different results for H and R_θ although they start from the same table of raw velocity data. This is especially important because entirely different methods of integration may have been used by the above-mentioned authors and this could lead to perhaps one half of the observed discrepancy between the results of different investigations shown in Fig. 14. At low values of H, the choice of mean curve near to the surface and in the extreme outer part of the profile is particularly important as the areas under these long 'tails' contribute proportionately more to the total areas to be integrated for δ^* and θ than at high values of H ($H > 2{\cdot}0$ say). This, however, cannot account for the spread of the values obtained in any individual investigation, as for instance, that of Hama alone, or of Smith and Walker alone, although the recent discovery of quasi-periodic spanwise variations of time-mean quantities in several layers that displayed no gross three-dimensional behaviour, may provide at least a partial explanation for this.

2.1.2. *Adverse pressure gradient* (Clauser*[6], Bauer[2], Stratford[64]).

Only Clauser's two layers have been used here, and as will be seen later, these do not appear to be accurately two-dimensional in spite of the care which was apparently taken in the experiments. Clauser's apparatus consisted of a slatted diffuser having a cross-section of low-aspect ratio, the boundary layer occupying a considerable proportion of the overall diffuser depth. Transition was forced by means of a wire approximately forty boundary-layer thicknesses upstream of the first measuring station.

The developments of H, and especially of R_θ (as shown in Figs. 1, 2, 15 and 16) exhibit a noticeable degree of irregularity, that was not removed by the recalculations undertaken by the present writer, and appears to exceed the level that might be expected due to purely random errors in measurement and data manipulation.

2.2. *Non-Equilibrium Layers on Flat Surfaces.*

2.2.1. Newman[37] carried out detailed measurements of mean velocity profiles, static pressure variation and the turbulence quantities u'^2, v'^2 and $\overline{u'v'}$ on the flat rear upper surface of a thick symmetrical aerofoil with the flow near separation at the trailing edge. Natural transition occurred behind the pressure minimum and free-stream turbulence was apparently small. The Series II boundary layer, although it has been used in later comparisons, again does not appear to be accurately two-dimensional. Velocity profiles are very detailed, and Reynolds numbers quite large.

2.2.2. Schubauer and Spangenberg[54] presented measurements of several boundary layers developing in their slatted diffuser and three of these layers, namely 'C', 'D' and 'E', have been used in this investigation. In order to force the boundary layer on the floor of their contraction out through a slot underneath the leading edge of their working wall (and thus to create a new boundary layer in which measurements could be made) they placed a gauze at the leading edge only twenty boundary-layer thicknesses (approximately) upstream of the first measuring station. Profile measurements are satisfactory, except close to the surface, but the values of H and R_θ become rather scattered, especially as separation is approached in distribution 'E' (*see* for example Fig. 6). Of these layers, only 'D' appears to be closely two-dimensional.

2.3. *Non-Equilibrium Layers on Curved Surfaces.*

2.3.1. Schubauer and Klebanoff[53] measured the turbulent boundary layer on a large simulated aerofoil in a wind tunnel having a circular cross-section. They obtained high Reynolds' numbers ($1500 < R_\theta < 77000$) and detailed velocity profiles up to separation, and for these reasons their data has been widely used to obtain the correlations required for various calculation methods although the values of R_θ and H (shown in Figs. 7 and 21) appear to be rather scattered, even after recalculation by the present author. The flow appears to be closely two-dimensional in the initial region of falling pressure. In the adverse pressure-gradient region, however, the flow becomes less accurately two-dimensional as separation is approached as indicated by the failure of their measured turbulence terms to account adequately for the rapid growth of momentum thickness in this region.

* Additional information relating to their investigations has been supplied by Prof. B. G. Newman, Dr. F. H. Clauser, and by Dr. G. B. Schubauer and their co-operation is gratefully acknowledged.

The surface has a convex curvature between $x = 0{\cdot}5$ ft and $x = 6{\cdot}0$ ft with a radius $R = 23$ ft, and also between $x = 16{\cdot}0$ ft and $x = 26{\cdot}0$ ft with $R = 31$ ft. For the measured layer $0 < \frac{\delta}{R} < 0{\cdot}024$.

2.3.2. von Doenhoff and Tetervin[13] carried out many measurements on various aerofoils at rather low Reynolds numbers. Their velocity profiles are not accurately defined and some care in the use of their data is required. Three layers were chosen for the present purposes, all of which were measured on an aerofoil designated NACA 65 (212)—222 (approx.) The layers corresponded to the conditions

$$R_c = 0{\cdot}92 \times 10^6, \qquad \alpha = 8{\cdot}1°.$$
$$R_c = 2{\cdot}64 \times 10^6, \qquad \alpha = 10{\cdot}1°,$$
$$R_c = 2{\cdot}67 \times 10^6, \qquad \alpha = 8{\cdot}1°.$$

The ranges of R_θ and δ/R were approximately,

$$750 < R_\theta < 1700; \qquad 0{\cdot}007 < \frac{\delta}{R} < 0{\cdot}023.$$

Transition was forced by a band of carborundum roughness extending from $x/c = 0{\cdot}025$ to $x/c = 0{\cdot}05$. The overall velocity profiles were, so far as could be ascertained, fully turbulent at the starting position for the calculations ($x/c = 0{\cdot}075$) which was only of the order of ten boundary-layer thicknesses farther downstream.

This aerofoil data has been extensively used as a basis for earlier calculation procedures because of the lack of alternative information. It still represents the most detailed investigation of aerofoil boundary layers except perhaps for the measurements of McCullough and Gault[36] and Altman and Hayter[1], which however appear to be rather scattered. (*See* Norbury[39]).

2.3.3. Schmidbauer[52] measured the developing layer on the convex wall ($R = 150$ cm) of a curved channel of rectangular cross-section with the unusual condition of initially rising and then falling pressure. Examination of the mean velocity profiles suggests that the natural transition is complete at $x = 46$ cm, which has been chosen as the starting point for the calculations described later.

The range of variables was approximately

$$1000 < R_\theta < 5000; \qquad 0{\cdot}007 < \frac{\delta}{R} < 0{\cdot}023.$$

The foregoing twelve measurements of boundary-layer development form the basis for the comparisons with experiment given in later sections.

3. *Methods of Calculating Momentum Thickness Development.*

3.1. *Calculations Performed.*

For all the experimental pressure distributions used in this investigation, step-by-step calculations of momentum thickness development have been carried out using the simple two-dimensional form of the momentum equation (7) together with experimental $H(x)$ values, and skin-friction values from a new relationship suggested by Sarnecki[49] which in fact gives values very similar to the familiar Ludwieg-Tillmann relation. These calculated results are compared with experiment in Figs. 1 to 10. Further calculations using modified forms of the momentum equation as given by Maskell[35], Truckenbrodt[71], Ross[44], and Rubert and Persh[47] are also shown for several cases. The results are presented as $R_\theta(x)$ because this is independent of arbitrary length scales and, in addition,

the Reynolds number gives some indication of the nearness of the boundary layer to transition conditions and hence whether the boundary layer is likely to be fully turbulent. The mean lines of experimental $H(x)$, $R_\theta(x)$ and the initial values used correspond to values of H and R_θ recalculated from the original velocity profile data given by the various authors.

3.2. *The Results of the Calculations.*

The first series of calculations, involving straightforward step-by-step integration of the momentum equation, reveal serious differences between the growth of R_θ as predicted by two-dimensional theory and that obtained in nearly all the experiments analysed, even far from separation.* This effect is important with regard to the prediction of shape-factor, as some auxiliary equations appear to be fairly sensitive to the assumption for $R_\theta(x)$ that is used in a calculation. As found in previously published comparisons, most of the calculated developments lie below the experimental values (*e.g.* Clauser II, Newman II, Schubauer and Spangenberg 'E', von Doenhoff and Tetervin aerofoil boundary layers, and Schubauer and Klebanoff (adverse pressure-gradient region)). However, the zero-pressure-gradient layer, assuming the mean line suggested by Coles[7], and the layers of Schmidbauer, and Schubauer and Spangenberg 'D' appear to be reasonably two-dimensional, whilst marked deviations in the opposite direction are shown for Clauser I and Schubauer and Spangenberg 'C'.

The remaining calculations may be divided into two groups:

(a) Step-by-step calculations using equation (7) but with extra terms added nominally to account for the influence of the normal turbulent stresses (*e.g.* Rubert and Persh[47]).

(b) Quadrature or algebraic solutions obtained by several authors, using experimental correlations to eliminate the explicit effects of H and c_f (*e.g.* Truckenbrodt, Ross, etc.).

In all cases (a) yields a more rapid rise of R_θ in adverse pressure gradients than the two-dimensional theory with turbulence terms neglected but gives no systematic improvement in the level of agreement with experiment, giving a rate of growth which is too large for Schubauer and Spangenberg 'D', Fig. 5, but too low in the case of Newman II, Fig. 3.

The calculations (b), performed by quadrature, spread widely about the two-dimensional result, with Truckenbrodt usually lower, and Maskell, Spence in agreement or larger. Again no definite relationship to experiment is observed for the selected cases shown in Figs. 1 to 4. The algebraic form given by Ross is appropriate to severe adverse pressure gradients and predicts very large R_θ values for the cases of Clauser I, Fig. 1, and Schubauer and Spangenberg 'C' and 'D', Figs. 4 and 5, but is quite good for Clauser II and Newman II, Figs. 2 and 3, where the experimental R_θ values exceed those of the two-dimensional results.

3.3. *Discussion of the Results of the Step-by-Step Calculations Using the Simple Momentum Equation.*

The disagreement between experiment and the two-dimensional theory might be attributed to any of the following causes:

(1) The inaccuracy of the skin-friction law used.

(2) The omission of terms involving the normal Reynolds stresses and terms involving the static pressure gradient normal to the surface.

(3) A departure from two-dimensional flow in these experimental boundary layers.

* The results of an earlier investigation by Coles[8] would lead to the same conclusions but are somewhat obscured by the method of presentation.

(1) Cannot explain the large discrepancies observed in Figs. 1, 2 and 3 unless the skin-friction law were in error by at least 100 per cent, which for either the new law or that of Ludwieg-Tillmann is very unlikely except for the very low values, close to separation, where the term involving c_f is negligible in comparison to the pressure-gradient term. Fig. 11 shows that for the layers of Clauser I and Newman II, quite unreasonable values of skin-friction are needed if the experiments are supposed to be two-dimensional, The slope of the curve of $\int_{xi}^{x} \frac{c_f}{2}\,dx$ (left as an integral to minimise calculation errors) is *negative* for Clauser I, if calculated from the two-dimensional equation, a negative value of skin friction therefore being required to give agreement with experiment. The new skin friction-law due to Sarnecki predicts quite plausible values, giving very small c_f for Newman at $x = 5{\cdot}0$ ft, under near separation conditions.

(2) Was thought to be the explanation by Ross[44], and Rubert and Persh[47], following Bidwell[3] and Goldschmied[21] who used the hot-wire measurements of Schubauer and Klebanoff to calculate these extra terms near to separation. The contributions of the measured terms obtained in the above experiment, and also as found by Newman[37], are shown in Figs. 7 and 3, respectively, from which it may be concluded that this is an incomplete explanation of the discrepancy in $R_\theta(x)$.

(3) Appears to be the real explanation, as was suggested by Tillmann when discussing the experiments of Weighardt and Tillmann[73], Ludwieg and Tillmann[33] and Kehl[30], who all used diffusers of a rectangular cross-section. These were of low aspect ratio and the boundary layers formed an appreciable portion of the whole flow. This leads to strong secondary flows which might also be expected to be present in the layers of Schubauer and Spangenberg, and also Clauser. Clauser[6] supports this conclusion after finding, in addition, the effect of instrument errors in his strongly turbulent conditions to be small. Norbury[40] in a thorough series of diffuser measurements also found strong three-dimensional effects on dR_θ/dx. The evidence thus suggests that most of the available supposedly two-dimensional experimental boundary layers are in fact three-dimensional with (usually) larger rates of growth indicating convergent flow. Two cases, Figs. 1 and 4, as already mentioned, exhibit divergent characteristics, a feature which does not appear to have been noted previously in the literature.

Where the geometry of the external streamlines can be specified then an approximate allowance for the secondary flow can be made and several authors have attempted to do this, Kehl for wedge flows and Norbury[39] for the flow in a plane of symmetry of his diffuser, but in general there is a component of the local velocity in the boundary layer normal to the tangent of the curved external streamline, and no direct measurements are available which are wholly suitable for testing calculation methods. This problem of cross-flow will be dealt with in a later report in connection with proposed new auxiliary equations.

3.4. *Discussion of the Results Obtained by Using Alternative Forms of the Momentum Integral Equation.*

Various authors have used the two-dimensional equation (7), solving it simultaneously step-by-step with their auxiliary equations, in conjunction with different assumptions for the skin-friction. We shall briefly discuss the particular assumptions made by these authors.

Gruschwitz[23] found that a constant value of $c_f = 0{\cdot}002$ gave acceptable results for his rather small range of H, R_θ.

von Doenhoff and Tetervin[13] used Squire and Young's formula,

$$c_f = 2[5{\cdot}890 \log_{10}(4{\cdot}075\ R_\theta)]^{-2}, \tag{11}$$

thereby neglecting any dependence of c_f on H.

Garner[20] used Falkner's expression, which similarly neglects dependence on H, thereby leading to large c_f values near separation. This procedure has been justified as making an allowance for the neglected turbulence terms in the equation but it is an arbitrary procedure which can scarcely be recommended.

Head[25] used the Ludwieg-Tillmann law which is generally satisfactory, and Kawasaki[29] assumed a very similar relationship obtained from Coles' profile family.

Rubert and Persh[47] added an extra term to equation (7), which became

$$\frac{d\theta}{dx} = \frac{c_f}{2} - \frac{\theta}{U_1}\frac{dU_1}{dx}(H+2) + \frac{\tau R}{2q}, \tag{12}$$

where $\tau R/2q\,[= f(\theta\, dH/dx)]$ was an empirical allowance for the turbulent normal stress terms. This is not generally satisfactory as demonstrated by Fig. 3, which shows the difference between this equation and the two-dimensional result with addition of measured turbulence terms for Newman II. In fact, it seems reasonable to conclude that it effectively attempted to allow for the lack of two-dimensionality of the experimental layers analysed (Schubauer and Klebanoff, Wieghardt and Tillmann, von Doenhoff and Tetervin). Regardless of its interpretation, however, it is clear that this equation cannot account for the existence of two-dimensional results lying above experiment in Clauser I, and below experiment in the case of Clauser II, as in both these layers, dH/dx is negative.

Ross[44] followed Dryden[14] in attempting to take account of the normal stress term in the momentum equation. He used the data of Schubauer and Klebanoff[53] and Granville's assumption that

$$\int_0^\delta \frac{\tau}{\rho U_1^2}\, dy \propto \delta^*,$$

to obtain the following form of the momentum integral equation,

$$\frac{d\theta}{dx} = \frac{\frac{c_f}{2} + (2+0{\cdot}97H)\Gamma_1 + 0{\cdot}016\,\theta\frac{dH}{dx}}{1 - 0{\cdot}016H}. \tag{13}$$

This equation is simplified by Ross for both large and for small pressure gradients. In the latter case equation (13) becomes

$$\frac{d\theta}{\theta} = \frac{dU_1}{U_1}\left[(H+2) + \frac{c_f}{2} - 0{\cdot}016\frac{dH}{dU_1}\right], \tag{14}$$

whilst for large pressure gradients he finds that, for the convergent data of von Doenhoff and Tetervin, Gruschwitz and Weighardt and Tillmann $\left(\text{if } \frac{\Gamma_1}{c_f} > \frac{1}{4}\right)$,

$$H + \frac{c_f}{2} - 0{\cdot}016\,\theta\frac{dH}{dx} = G \approx 2{\cdot}8. \tag{15}$$

Thus, by fitting a straight mean line to the rather scattered data on the log-log plot shown in Fig. 12, he obtained the simple expression

$$\frac{\theta}{\theta_i} = \left(\frac{U_{1i}}{U_1}\right)^{2+G}, \qquad (i \text{ denotes initial position}).$$

An attempt to improve accuracy is made by expressing G as a function of initial R_θ $(= R_{\theta i})$, but as seen in Fig. 13 there is considerable scatter about the curve chosen. This method cannot be considered to be a reliable representation of all the data used in these correlations, and in fact discrepancies of up to $\pm$ 20 per cent are seen in Fig. 12 and of $\pm$ 16 per cent in Fig. 13. No direct comparisons with experiment are given by the author who states however that 'The (calculated) results should usually be accurate to within about $\pm$ 10 per cent'. This statement is scarcely borne out by the results of calculations presented in Figs. 1, 4 and 5, although quite good agreement with experiment is seen in Figs. 2, 3 and 10. The condition $\Gamma_1/c_f > 1/4$, restricts application to the ranges of x shown, and to $x > 19$ ft for Schubauer and Klebanoff.

The remaining methods to be considered are all derived from equation (7) with no explicit allowance for any turbulence terms or three-dimensional effects. By the use of suitable assumptions equation (7) is reduced to a directly integrable form for θ as a function of $U_1(x)$.

Putting $c_f = \dfrac{\alpha}{R_\theta^{1/n}}$, and H = constant, equation (7) becomes

$$\frac{d}{dx}(\theta R_\theta^{1/n}) = \frac{n+1}{n}\alpha - \left[2 + \frac{1}{n} + \frac{n+1}{n}H\right]\frac{\theta R_\theta^{1/n}}{U_1}\frac{dU_1}{dx}, \tag{16}$$

which integrates to give

$$\theta R_\theta^{1/n} = U_1^{-d}\left[c_1 + c\int_{x_1}^{x} U_1^{d}dx\right], \tag{17}$$

where

$$d = \frac{n+1}{n}H + 2 + \frac{1}{n},$$

and

$$c = \frac{n+1}{n}\alpha.$$

The values of c and d thus depend on the skin-friction law and (constant) value of H assumed.

The original attempt by Buri[5] to calculate the turbulent boundary layer using an analogous approach to that of Pohlhausen[42] for the laminar layer involved the assumptions

$$c_f = \frac{f_1(\Gamma)}{R_\theta^{1/n}},\ H = f_2\,(\Gamma \text{ only}), \qquad \text{where} \qquad \Gamma = \frac{\theta R_\theta^{1/n}}{U_1}\frac{dU_1}{dx}.$$

He found by experiment that $d(\theta R_\theta^{1/n})/dx = F(\Gamma) = c - d\Gamma$ for a limited range of data and was thus able to integrate the momentum equation in the form (17).

In view of the use of an empirical correlation for $F(\Gamma)$ the method does not assume a unique dependency of profile shape on local pressure gradient as far as momentum thickness prediction is concerned.

Maskell's[35] treatment is less restrictive and involves the transformation of equation (7) in a manner suggested by the Ludwieg-Tillmann skin-friction formula. He uses more comprehensive experimental data than Buri and matches the Ludwieg-Tillmann results for boundary-layer develop-

ment in zero pressure gradient. Empirical correlations are shown only for $1{\cdot}2 < H < 2{\cdot}0$ and, whilst these appear to be satisfactory at first sight, they are based entirely upon measurements in convergent layers, although the less reliable measurements on the nose-opening aerofoil of von Doenhoff and Tetervin are not matched closely. The results shown in Figs. 1 and 4 reveal the more rapid rise of calculated R_θ compared to two-dimensional theory, as may be expected for a method matched to convergent flow, although better agreement is found in Fig. 2.

Truckenbrodt[71] (1952) used the energy integral equation (6) with Rotta's[45] analysis of the data of Ludwieg-Tillmann and Schultz-Grunow for the dissipation integral. (Assuming no contribution of the flux of turbulence energy, this is equal to the shear-stress work integral $\int_0^\delta \frac{\tau}{\rho U_1^2} \frac{\partial \left(\frac{u}{U_1}\right)}{\partial y} dy$). He thus obtained a similar quadrature form to (17) the approach being only formally different (as remarked upon in his Appendix).

However, Rotta's treatment allowed for three-dimensional effects in the boundary layers considered, as described later in Section 4.5.4, and should therefore be used in conjunction with the corresponding three-dimensional form of the energy equation. The fact that this was not done means that the empiricism in Truckenbrodt's derivation might again be influenced by three-dimensional effects. His correlations are however difficult to comment upon as no experimental points are shown.

His calculation seems to predict lower values of R_θ than are obtained from the two-dimensional theory, Figs. 1, 2 and 4, and this may indicate that a form of the quadrature equation could be arranged to agree with the two-dimensional results. The saving in computational labour may not be important, however, especially if a digital computer is available.

Spence[61] after summarising the quadrature methods (including his own, which again used different values of c and d), considered (as did Ross) that the appeal to experiment effectively allowed for the normal-stress terms and he suggested that there was little to choose between the different versions, all being quite satisfactory. The evidence presented here does not support this conclusion and the results given by Spence's own equation are in fact usually higher than the two-dimensional result, as shown in Figs. 1 and 4.

3.5. *Conclusions.*

The use of any of the empirically modified equations can scarcely be justified, as, whilst containing no explicit allowance for secondary flows, they have been matched largely to results obtained in convergent flow and are therefore incapable either of predicting the growth correctly in a divergent flow (as seen in Figs. 1 and 4) or of allowing for the range of cross-flow that is possible with a given external pressure distribution. On engineering grounds, if the restriction to convergent or two-dimensional flow is specified the results might be of value, but an attempt to correlate the extent of cross flow with such factors as the aspect ratio of the duct in which the layer is developing, and the ratio of boundary-layer thickness to duct dimensions might be of more use in obtaining a correction to the two-dimensional equation. More measurements of turbulence and static pressure effects are needed as well as a more complete knowledge of the three-dimensionality of the flow in order to evolve accurate calculation techniques.

Kehl's equation is of use only when the external streamlines are nearly straight, but has been adopted by Rotta when using the energy integral equation to make approximate corrections to some earlier German data.

The addition of turbulence terms to the equation (7) in layers developing towards separation seems always to increase dR_θ/dx whereas secondary-flows may either increase or decrease dR_θ/dx. Thus no empiricism on the grounds of allowing for turbulence effects, in order to fit experimental results, is justified.

4. *Methods of Calculating Shape-Factor Development.*

4.1. *The Basis for Comparisons of Shape-Factor Calculations.*

4.1.1. *The choice of momentum thickness distribution.*—The calculation of shape-factor can be based upon the momentum thickness obtained from

(i) two-dimensional theory {equation (7)},

or (ii) the empirically modified form of equation (7) appropriate to a particular complete calculation method,

or (iii) experimental measurements.

In predicting boundary-layer development for new circumstances where no experiments are available, then strictly two-dimensional conditions may be assumed and (i) is the correct choice, including second-order terms near to separation.

If the complete calculation procedures of different authors are to be compared then the appropriate example of (ii) must be used.

For the purposes of the present investigation, the predictions of the auxiliary equations were to be compared with measured shape-factor developments as well as with each other.

If calculations are carried out on the basis of $U_1(x, z_i)$, H_i and $R_{\theta i}$ alone, then no information concerning the nature of any real secondary flows, which appear to be present in the measured layers considered here, is incorporated in the calculation and there is no reason to expect that the use of (i) or (ii) will give satisfactory results unless the calculated $H(x)$ is very insensitive to the choice of $R_\theta(x)$*. Consequently it is only possible, in the absence of direct measurements, to take some account of the real three-dimensional character of the flow by using the appropriate experimental R_θ development as a basis for the shape-factor calculations. This is necessary because a family of secondary flows could be associated with the given boundary values $U_1(x, z_i)$, H_i and $R_{\theta i}$ and each of the members of this family would give rise to a particular combination of $R_\theta(x, z_i)$ and $H(x, z_i)$. Hence, in order to predict $H(x)$ correctly, the corresponding $R_\theta(x)$ development must be used, and not some other (*e.g.* the 'two-dimensional') values that are appropriate to a different member of the family of possible flows.

The third alternative, of using experimental $R_\theta(x)$, has thus been adopted in this investigation to judge the relative merits of existing equations. It is not suggested that it can provide more than an approximate account of the lack of agreement with the idealised two-dimensional flow, but it appears to be the only satisfactory procedure until more detailed measurements become available.

It is also assumed that the velocity profile family and the skin-friction law are not too greatly affected by the presence of secondary flows. This is the usual assumption for the streamwise

---

* This is only true for a few auxiliary equations (for example Spence, Rubert and Persh) in which a dependency of the various coefficients, on H alone, is assumed for the sake of simplicity. The more reliable equations (such as Head[25]) give results which depend noticeably on the assumed distribution of $R_\theta(x)$, as seen in Figs. 36 and 37. Further consideration of this point is given later, in Section 4.6.

properties in a three-dimensional layer and is well supported by the results of comparisons carried out by the present author, between a new two-parameter profile family and measured profiles.

Fortunately, where many comparisons are to be made, the use of (iii) constitutes the simplest numerical technique, and for this reason it has been used previously, without any attempt at a direct justification, by Norbury[39] and by Head[25], as the basis for comparing their equations with experiment.

4.1.2. *The choice of initial values.*—

(i) For the present purpose of comparing auxiliary equations with experiment, and in general for testing or calibrating a new auxiliary equation, the initial values of H and R_θ are taken from experiment.

(ii) For full calculations in new circumstances where no experiments are available, a laminar solution is normally used with an assumed sudden transition specified by some empirical rule. R_θ is assumed to be continuous and is thus known, the problem being to calculate the fall in H value at transition so that at the end of the physically real transition zone the turbulent solution will proceed correctly downstream. Again, various empirical rules are available, but are not generally satisfactory.

In either case, an uncertainty exists as to the correct choice of starting values for $H(= H_i)$ and for $R_\theta\ (= R_{\theta i})$.

To check that transition was complete for the chosen initial conditions measured profiles were compared with a new two-parameter family which will be described in a subsequent report. Where overall agreement between the calculated and experimental profiles was obtained, and where, in addition, the inner portion of the experimental profile agreed with the assumed universal wall law, the influence of transition was assumed to be negligible, as a definite family of inner and outer profiles was satisfied which contained no explicit reference to the transition conditions.

Even when the most upstream position permissible for starting a calculation is found, the actual value of H_i is uncertain, due to experimental errors and also due to errors in the manipulation of the data.

Recalculations of H and R_θ have been made for the velocity profiles of all the layers needed in this investigation, and as shown in Figs. 1 to 10, and Figs. 14 to 24, these values usually showed some disagreement with the values quoted by the original authors. The recalculated values were used throughout as they have been analysed by a consistent and, it is believed, accurate numerical procedure.

Ideally therefore, a comparison with experiment should cover the range of uncertainty in H_i ($R_{\theta i}$ is less critical), because, as is shown later, the calculations of $H(x)$ are often strongly dependent on the choice of initial conditions, particularly in severe adverse pressure gradients. A good auxiliary equation should give agreement with experiment for at least part of this range of H_i, but the degree of dependence of the solution on H_i is not yet fully understood, as the stability of the development of the real flow (where of course R_θ would be free to vary) to such disturbances is not yet known. Clauser[6] shows that in strong adverse pressure gradients the downstream flow may not recover from a sudden disturbance. Further discussion of this problem is given later where it is shown that several existing equations give predictions which depend to an implausible extent on H_i.

In the case of (ii), the uncertainty is more serious, especially for H_i, as transition behaviour has yet to be calculated. Whilst this problem is outside the scope of this investigation, some empirical rules for estimating H_i will be mentioned.

Truckenbrodt[71] suggests the relationship between transition Reynolds number ($R_{\theta t}$) and the fall in shape-factor, $\Delta H\,(= H_{\text{laminar}} - H_{t\text{turb}})$, from the calculated laminar value at transition. No justification is given from experiments, except for zero pressure-gradient conditions.

Maskell[35] tentatively proposed that

$$\Delta H = f\left[\frac{\theta R_\theta^{0\cdot268}}{U_1} \cdot \frac{dU_1}{dx}\right],$$

on the basis of a dimensional analysis for natural transition, in adverse pressure gradients for $R_\theta < 2500$. He suggests the use of flat plate values, that is $H_t = H_0(R_\theta)$, in favourable or zero pressure gradients. Various other authors (Spence[60, 61], von Doenhoff and Tetervin[13] have assumed the latter rule for all pressure-gradient conditions for want of a better assumption.

Garner[20] considered that $dH/dx < 0$ indicated incompletely turbulent flow but this supposition is not substantiated in the present report and, Maskell in particular, has disagreed.

Thus for new calculations a rule is needed for both transition position and ΔH. The following effects should be taken into account (and in fact may have affected Maskell's approach, as he included the data of von Doenhoff and Tetervin where forced transition was employed):

(a) The method of causing transition (*e.g.* laminar separation, natural transition on the surface, wire, serrated strip, surface roughness, air jets, etc.).

(b) The level of vorticity (turbulence) and non-uniformity of the free-stream.

(c) The pressure distribution over the finite length of the (real) transition.

4.2. *The Generalised Auxiliary Equation.*

The purely empirical equations of von Doenhoff and Tetervin[13], Garner[20], Maskell[35], Spence[61], and others; the energy equations of Truckenbrodt[71], Rubert and Persh[47], and Kawasaki[29], and the entrainment equation of Head[25] can be reduced to a generalised auxiliary equation discussed by Spence[61], who introduced it from shear-stress considerations. Truckenbrodt[71] had previously mentioned a similar analysis.

The generalised equation was written by Spence as

$$\Theta \frac{dH}{dx} = \Phi(H) \,.\, \Gamma - \Psi(H), \tag{18}$$

where $\Theta = \theta R_\theta^{1/n}$ and $\Gamma = -\dfrac{\Theta}{U_1}\dfrac{dU_1}{dx}$, with the value of n effectively determined by the skin-friction assumption used in each case.

It is now rewritten as

$$\theta \frac{dH}{dx} = \Phi(H) \,.\, \Gamma_1 - \frac{\Psi(H)}{R_\theta^{1/n}}, \tag{19}$$

where $\Gamma_1 = -\dfrac{\theta}{U_1}\dfrac{dU_1}{dx}$ and can be directly related to experiment since no explicit value of n is used.

The newer equations (Head, for example) necessitate the dependence of Φ, Ψ on R_θ also, and so the equation is used in the form:

$$\theta \frac{dH}{dx} = \Phi(H, R_\theta) \cdot \Gamma_1 - \frac{\Psi(H, R_\theta)}{R_\theta^{1/n}}, \tag{20}$$

i.e.

$$\theta \frac{dH}{dx} = P \cdot \Gamma_1 + Q. \tag{21}$$

This equation is a purely mathematical representation of the results of different analyses, and provides a concise summary of the comparative properties of different equations. It allows one to forecast, qualitatively, the relative behaviour of different equations under given circumstances, but the absolute level of agreement with experiment cannot be determined unless some direct calculations are first performed. It cannot reveal any of the physical or experimental details used in the derivation of any individual equations and so is quite unable to provide reasons for the form of the P, Q curves, shown in Figs. 25, 26 and 27.

Hence, whilst with experience of some selected calculations, it can save labour by forecasting the relative merit of different methods (and has been used to show in which range of H, R_θ the cause of apparently anomalous behaviour lies), it cannot suggest ways of improving agreement with experiment nor is it applicable in situations requiring the introduction of new variables, such as suction or blowing.

Thwaites[67] for Spence's[61] method, Head[25] and more recently Kawasaki[29], have shown limited comparisons of P, Q but without detailed discussion.

As will be shown later, the generalised form can be used to indicate the stability of various equations in unfavourable pressure gradients. In these conditions all equations will show divergent behaviour following a change in the initial H value (or an error in the calculated H value at some intermediate step) if the pressure gradient parameter Γ_1, exceeds a certain critical value appropriate to the equation concerned.

4.3. *The Shape-Factor Calculations.*

The selection of particular comparisons was not obvious in the initial stages, but the saturation of the problem by applying all proposed calculation methods to all experimental cases was obviously impracticable. Some of the earlier equations were rejected as being based on an insufficient range of accurate data and correlations, and some on the basis of published comparisons (for example, Spence showed the poor agreement given by von Doenhoff and Tetervin's method for Schubauer and Klebanoff's boundary layer).

Following a rather arbitrary selection of preliminary calculations in order to gain experience, a more comprehensive series of calculations was made, using the equations of Head[25], Spence[61], Maskell[35], Rubert and Persh[47] and Truckenbrodt[71]. Only Head[25] and Spence[61] have been applied to all the experimental cases considered. Consideration of the generalised coefficients P, Q of these equations allowed their relative behaviour to be estimated and only a few selected cases were calculated to check this and to bring out the particular idiosyncrasies of each approach. Other equations not included in this series of direct comparisons are however dealt with in section 4.5 and their relative usefulness can be estimated for similar conditions by considering their P, Q curves. In particular, the equations of Walz[72], and of Kawasaki[29] would appear on this basis to offer no

advantages, in their present forms, over Truckenbrodt for example. However, the equation of Gruschwitz[23] appears likely to yield results comparable to those of Head, but only for $H \leqslant 2{\cdot}0$; $R_\theta \leqslant 3000$.

Figs. 14 to 24 show the comparisons between calculated and experimental $H(x)$. The experimental H values given by the original authors are shown together with the recalculated values which are thought to be more reliable as a basis for the comparisons.

The experimental mean lines of $R_\theta(x)$ are shown in Figs. 1 to 10 and have been discussed already in Section 2.3.

Fig. 35 shows, for some of the equations, the effect of different H_i values on the calculated $H(x)$ development and will be discussed in Section 4.6. The influence of the assumptions for momentum growth on calculated $H(x)$ is indicated in Figs. 36 and 37, for two rather different auxiliary equations.

4.4. *Discussion of Results.*

All equations were applied to Clauser I and II, Figs. 15 and 16, because this data had not been used previously and was rather different in character from other measurements in rising pressure conditions, with very small variations in H. It was considered that these cases would provide a severe test of the equations. This established some general trends, which could be related to the P, Q curves of each equation, and which were further confirmed by the results shown in Fig. 17. The principal conclusion reached from an examination of Figs. 15, 16 and 17 is that, for $H > 1{\cdot}45$ and $\Gamma_1 > 0{\cdot}001$ (approximately), the predictions of the different equations, in order of descending dH/dx and hence of increasing accuracy, are: Spence, Maskell, and Rubert and Persh, Truckenbrodt, Head. (With the exception of the range of negative P for low R_θ and $H \approx 1{\cdot}6$, for Rubert and Persh, who then predict the lowest dH/dx).

This result is due to the relative magnitude of the P coefficients in the generalised form which multiply the pressure gradient parameter (Γ_1) and tend to raise dH/dx in rising pressure conditions.

P falls off progressively in the order:

Maskell $\left(\text{large } \Gamma, \text{ where Maskell defines } \Gamma = \dfrac{0{\cdot}246}{c_f}\dfrac{\theta}{U_1}\dfrac{dU_1}{dx}\right)$, Truckenbrodt, Rubert and Persh ($R_\theta = 10^5$), $\left.\begin{matrix}\text{Head}\\ \text{Spence}\end{matrix}\right\}$, Maskell (small Γ), and Rubert and Persh ($R_\theta = 10^3$).

The Q term $\left[= \left(\theta \dfrac{dH}{dx}\right)_{\Gamma_1=0}\right]$ in all cases tends to lower $\dfrac{dH}{dx}$ and thus opposes the effect of P.

Q is very small for Spence and for Rubert and Persh, and thus their calculated values of dH/dx are seen to be much too large, except where $P < 0$ for Rubert and Persh.

Head's value is much larger and, in conjunction with a similar P value to that of Spence, accounts for the prediction of much lower values of dH/dx.

Truckenbrodt and Maskell by similar arguments can be seen to be intermediate in behaviour.

The remaining cases were calculated using the equations of Spence[61] and Head[25], which usually represent the upper and lower limits to calculated $H(x)$, as indicated by the above. However, for Schubauer and Klebanoff, and Schubauer and Spangenberg 'C', 'D' and 'E', the calculations start below $H = 1{\cdot}45$, in a region where the relative magnitudes of P, Q of different equations have changed (again refer to Figs. 25, 26 and 27).

Typical predictions of H in this range showed that Head now gives an unreasonably large rate of growth of H in adverse pressure gradients, whilst Spence now shows the least tendency to rise.

The other methods also change their relative behaviour in this range if Γ_1 is large enough. For example, if $H < 1{\cdot}4$ for all R_θ, Rubert and Persh show an excessive variation of H with Γ_1, but for $H \geqslant 1{\cdot}4$, the behaviour depends critically upon R_θ. The behaviour at larger H, R_θ values will produce a trend towards the same relative order of separation prediction as described for the earlier cases although this is not quite achieved in Fig. 19.

Two unexpected results should be noted:

(1) If Spence's calculation is started in a favourable pressure gradient, the calculated H falls as expected, rather rapidly since $P > 0$, but, in contrast to Head, $Q < 0$ (for $H < 1{\cdot}4$) and this depresses H as well, almost asymptotically towards $H = 1{\cdot}21$ where $P = 0$ and Q is very small and thus $\frac{dH}{dx} \approx 0$. This is clearly shown in the calculated result starting at $x = 1$ ft for Schubauer and Klebanoff, Fig. 21, and this further demonstrates that as $P = 0$, no subsequent adverse pressure gradient can raise H again.* Because of the large value of P for $H < 1{\cdot}4$, the method of Rubert and Persh will be poorer than that of Spence in this example.

(2) Fig. 24 shows the result of applying Maskell's method to the experimental data of Schmidbauer[52] where the pressure gradient changes from adverse to favourable in the course of the boundary-layer development. After a rather rapid rise of H in the adverse pressure-gradient region, the use of $H = H_0(R_\theta)$ as proposed by Maskell for all favourable pressure-gradient regions, causes a discontinuity in the predicted $H(x)$ to appear at $x = 110$ cm where the pressure gradient changes sign.

Finally, the flat-plate zero pressure-gradient results of the different methods are compared to Coles' similarity solution in Fig. 14. The large scatter of experimental $H = H_0(R_\theta)$ values is clearly shown, although it should be remembered that the scale of H is larger than in the other figures.

The discussion of these results will be continued during a chronological review of the different auxiliary equations which are now classified either as being purely empirical or in terms of their physical basis.

The following points may be mentioned at this stage; the wide range of predictions shown by the use of different equations for any experiment considered; the generally reasonable agreement with experiment given by Head but the indifferent to very poor agreement given by the other equations, except for the data of von Doenhoff and Tetervin, Figs. 22 and 23, which had in many cases been used in obtaining the original correlations. However, the newer measurements of Clauser and Newman are not well represented even by Head's equation which is, nevertheless, rather better than the remainder.

Rotta[46] has compared a large number of auxiliary equations in terms of the coefficients of the generalised form and confirms, independently, the present results which show the striking differences between many of the existing equations. However, Rotta shows no direct comparisons between calculated H development and experiment, mainly confining his treatment to an approximate analysis of 'equilibrium' conditions, where $dH/dx = 0$ and a mean value of $R_\theta = 10^4$ was assumed (*see* his Fig. 22.1). This approach, however, leads to the erroneous conclusion that Head's equation will predict accurately, the shape-factor development for Clauser II (in contrast to the result shown in Fig. 16), although it clearly agrees with the present conclusions regarding the very

* It should be remembered in connection with this example, that Spence started his calculation at the beginning of the adverse pressure gradient region, Fig. 21, giving a good separation prediction. This further demonstrates the need to calculate as many cases as possible and to study the forms of proposed P, Q curves.

poor performance of the majority of the other equations under these conditions. For non-equilibrium layers, it is difficult to draw any definite conclusions from Rotta's analysis although his general remarks concerning the difficulties of shape-factor calculation are in agreement with the conclusions of the present investigation.

4.5. *A Review of Existing Auxiliary Equations and Further Discussion of the Comparisons with Experiment.*

The earlier methods, although not used in the present calculations, are described, as they show the order in which the physical features of the flow were appreciated. Difficulties encountered in obtaining quantitative relationships from experimental data are also shown clearly by these earlier attempts and enable general conclusions to be drawn which also apply to more recent investigations.

4.5.1. *Early empirical equations* (1930-1943).—As already mentioned, the first attempt at a complete calculation procedure was made by Buri[5] by analogy with the method for laminar flow due to Pohlhausen[42]. Buri's method can be seriously considered only as a method of calculating R_θ; the assumption that Γ is a form parameter is inadequate as it effectively requires that the surface boundary condition $(\partial\tau/\partial y)_0$ specifies the complete (local) distribution of shear-stress, and further, that this specifies the local velocity profile completely. This neglects the finite time taken for the outer part of the boundary layer to feel the influence of surface conditions.

Buri's assumptions appear to work over a limited range of his favourable pressure gradient data but required modification to fit the diffuser experiments of Nikuradse[38].

Gruschwitz[23] recognised that the pressure gradient does not determine the local velocity distribution but only controls its rate of development, and derived the following auxiliary equation by considering the energy exchange at $y = \theta$;

$$\frac{\theta}{q}\frac{dg_1}{dx} = F(\eta, R_\theta).$$

In this equation, which is obtained from dimensional arguments,

$$\eta = 1 - \left[\left(\frac{u}{U_1}\right)_{y=\theta}\right]^2 = \frac{g_0 - g_1}{q}. \tag{22}$$

q = local free stream dynamic pressure,
$= \frac{1}{2}\rho U_1^2$,
g_0 = free stream total pressure,
g_1 = total pressure at $y = \theta$.

is the chosen form parameter, *i.e.* $\dfrac{u}{U_1} = f\left(\dfrac{y}{\theta}, \eta\right)$.

From somewhat limited experimental data Gruschwitz found a linear dependency of F on η only, *i.e.* for $250 < R_\theta < 4500$; $1{\cdot}2 < H < 2{\cdot}0$,

$$\frac{\theta}{q}\frac{dg_1}{dx} = -\frac{\theta}{q}\frac{dq\eta}{dx} = A\eta - B,$$

or

$$\theta\frac{d\eta}{dx} = -\left[A + 2\frac{\theta}{U_1}\frac{dU_1}{dx}\right]\eta + B, \tag{23}$$

where $A = 0{\cdot}00894$ and $B = 0{\cdot}00461$.

However, Kehl[30]* showed that B depended upon R_θ, and from an analysis of his much wider range of very careful measurements obtained the following relation:

$$B = \frac{0{\cdot}0164}{\log_{10} R_\theta} - \frac{0{\cdot}85}{R_\theta - 300} \tag{25}$$

for $\qquad 250 \leqslant R_\theta \leqslant 35000\,; \qquad 1{\cdot}1 \leqslant H \leqslant 1{\cdot}8\,.$

Further, he showed, Fig. 28, that a singly infinite family of velocity profiles is not a good assumption, his new results generally disagreeing markedly with the mean line chosen by Gruschwitz. This is a clear example of the frequently observed inability of a purely empirical approach to extrapolate beyond the range of the original data.

Schmidbauer[52] adapted the Gruschwitz method to account for different rates of boundary-layer growth due to convex curvature of the surface in a streamwise direction.

He obtained good agreement with his own experimental R_θ, η distributions on the basis of two empirical correlations, supported by physical arguments concerning the change in turbulent mixing due to flow curvature.

He calculated c_f {from the momentum integral equation (7)} and found

$$c_f = f(\theta/R) \text{ only}, \qquad \text{for} \qquad 0{\cdot}001 \leqslant \theta/R \leqslant 0{\cdot}004,$$

where R is the radius of curvature of the surface. He neglected the effects of H, R_θ, as had Gruschwitz when calculating $R_\theta(x)$.

The auxiliary equation (23) was modified to incorporate a dependency upon θ/R, and whilst this may be quite acceptable on physical grounds, the significant variation of skin-friction with θ/R is very similar to the change that would be expected on a flat surface if the variation with H is allowed for, using any one of the accepted relationships found later such as that of Ludwieg and Tillmann. Furthermore, if Schmidbauer's velocity profiles are checked on a Clauser plot a reasonably well defined logarithmic inner profile is found, corresponding to these skin-friction values, with no need to postulate any effect of wall curvature, and it can in fact be shown from other experimental results that the overall velocity profiles are not likely to be appreciably affected by wall curvature for

$$|\theta/R| \leqslant 0{\cdot}004\,.$$

---

* Kehl made the first measurements for convergent or divergent radial flows with various pressure distributions. He presented the appropriate form of the momentum equation for this type of flow, namely

$$\frac{d\theta}{dx} = \frac{c_f}{2} - (H+2)\frac{\theta}{U_1}\frac{dU_1}{dx} - \frac{\theta}{(x+x_0)}\,, \tag{24}$$

where $(x+x_0)$ is the distance along the plane of symmetry measured from the virtual origin of the radial flow.

Owing to the growth of the side wall boundary layers, and the sudden start of the wedge-flow region there is some slight extra secondary flow associated with the curvature of the external streamlines, not accounted for by the term $\dfrac{\theta}{(x+x_0)}$, as pointed out by Wieghardt and Tillmann[73]. The nature and magnitude of these cross-flows was thought by Kehl not to have affected the overall streamwise velocity profile shape or the form of the auxiliary equation. As mentioned above, he successfully made a new correlation in terms of R_θ and thereby avoided the need to start his shape-factor calculation at the artificially low value $\eta = 0{\cdot}1$, in the transition region. This had been an objectionable feature of the Gruschwitz method.

For his comparatively restricted range of measurements, it therefore seems probable that the values of H and θ/R were fortuitously correlated; the larger H values being associated with larger θ/R and hence his lower c_f values.

This illustrates the importance of clear physical understanding and the use of enough experimental information to allow separation of the effects of different variables before correlating data.

4.5.2. *Later empirical equations of von Doenhoff and Tetervin, Garner, and Maskell.*— von Doenhoff and Tetervin[13], were able to derive an improved auxiliary equation using, in particular, their own newly available series of measurements of boundary-layer growth on aerofoils. Again, in contrast to Buri, they correlated rate-of-change of shape-factor against local pressure gradient. They also introduced a dependency on H, yielding

$$\theta \frac{dH}{dx} = f\left[-\frac{\theta}{q}\frac{dq}{dx}\frac{2q}{\tau_0}, H\right]. \tag{26}$$

Their correlations for $H \leqslant 1{\cdot}4$ are not completely satisfactory, Fig. 29, and in addition no direct measurements in favourable or zero pressure gradient were employed; their assumption of the 1/7th power law profile for these conditions may also lead to some inaccuracy. Their equation was

$$\theta \frac{dH}{dx} = e^{4{\cdot}68(H-2{\cdot}975)}\left[-\frac{\theta}{q}\frac{dq}{dx}\frac{2q}{\tau_0} - 2{\cdot}035\,(H-1{\cdot}286)\right] \tag{27}$$

where, for $dq/dx = 0$, $H = H_0$ and tends towards the limiting value $1{\cdot}286$.

Skin-friction values were obtained from the well-known Squire-Young relationship (11).

They presented the first explicit profile family, based on the one parametec H, *i.e.*

$$\frac{u}{U_1} = f\left(\frac{y}{\theta}, H\right), \qquad \text{for} \qquad 1{\cdot}286 \leqslant H \leqslant 2{\cdot}6. \tag{28}$$

This was presented as a contour plot of their measurements, which covered only a small range of R_θ, except for the nose-opening aerofoil data which they acknowledged to be somewhat unreliable due to secondary flows.

They briefly considered the effects of different initial values.

Garner[20] re-analysed the same data using Falkner's skin-friction formula, and obtained a simpler analytic form for the auxiliary equation with the assumption that, for $dq/dx = 0$, H tended towards the limiting value $1{\cdot}4$.

For the case $dH/dx = 0$, Fage and Raymer[17] obtained very different results when comparing these two methods and attributed this to an insufficient range of data used in obtaining the original correlations.

The equation of Maskell[35] is the first of the existing equations considered in the calculations presented above.

Maskell wrote his equation in a similar form to that of von Doenhoff and Tetervin, *i.e.*

$$\theta R_\theta^{1/n}\frac{dH}{dx} = \Phi(\Gamma, H), \qquad \text{where} \qquad \Gamma = \frac{0{\cdot}246}{c_f}\frac{\theta}{U_1}\frac{dU_1}{dx}$$

The earlier difficulties in wholly zero pressure-gradient conditions were avoided by matching the distribution of $H = H_0(R_\theta)$ to experimental values given by Ludwieg and Tillmann[33]. Hence

$$\Phi(0, H) = \Phi(0, H_0), \qquad \text{for} \qquad H < 1{\cdot}4; \qquad 10^3 < R_\theta < 4 \times 10^4.$$

Outside this range, the function $\Phi(0, H)$ was derived by extrapolating to $\Gamma = 0$ the correlations for adverse pressure-gradient data which took the form

$$\Phi(\Gamma, H) = \Phi(0, H) + \Gamma \cdot g(H).$$

Two such linear relationships were needed, one for large values of Γ, ($\Gamma > \Gamma_i$), the other for small values of Γ ($\Gamma < \Gamma_i$), the changeover function $\Gamma_i = \Gamma_i(H)$, being given from experiment. (The suffix i in this case is Maskell's own notation and does not here refer to initial conditions).

The correlations for $\Phi(\Gamma, H)$ are shown only for $1{\cdot}4 \leqslant H \leqslant 1{\cdot}9$ and exhibit considerable scatter due to the graphical differentiation employed. The choice of a non-linear overall variation of dH/dx with pressure gradient is less restrictive than the assumption used in other empirical equations and is suggested by the form of the von Doenhoff curve at low H, Fig. 29, but the best choice of relationship is not immediately obvious and any assumed curve can be justified only by the results of direct calculations. The correlation at large Γ depends entirely upon the possibly inaccurate nose-opening aerofoil data of von Doenhoff and Tetervin, and in fact the only new measurements used are those of Schubauer and Klebanoff[53].

$\Phi(0, H)$ and $\Gamma_i(H)$ were shown only for $1{\cdot}25 \leqslant H \leqslant 1{\cdot}7$ and in the present calculations it has been necessary to extrapolate to considerably higher H values, which may explain the rather poor results in certain circumstances.

For all zero or favourable pressure-gradient conditions, regardless of the previous history of the layer, this approach assumes that $H = H_0(R_\theta)$ from Ludwieg and Tillmann's flat plate results.*

As already shown in Fig. 24 this causes a discontinuity in the predicted $H(x)$ if the local pressure gradient changes sign, and again emphasises that the local pressure gradient cannot specify the whole velocity distribution at that position.

The comparisons in Figs. 15, 16, 17 and 19 show that Maskell's equation predicts excessive dH/dx values in rising pressure conditions, leading to the unacceptably early separation predictions shown. Consideration of Maskell's own Figs. 3, 4 and 5 and 10, 11 and 12 indicates that if his calculations were repeated for the experimental H_i values used in the new calculations of von Doenhoff's aerofoil layers, and if experimental $R_\theta(x)$ was used throughout, for both his calculations and those of von Doenhoff and Tetervin, then his results would generally be poorer than those of the latter authors and would predict as usual, an early separation.

However, the excellent result for Schubauer and Klebanoff, confirmed in Fig. 21, would appear to indicate that Maskell's approach is better than the earlier one, for larger values of R_θ. A study of the P, Q curves suggests that for $H > 1{\cdot}8$, von Doenhoff's equation predicts an excessive variation of H with pressure gradient and is unsatisfactory in showing little dependency on R_θ.

All these purely empirical equations suffer from the need to rely upon rather scattered direct correlations which are, in the absence of any physical guidance, open to a range of alternative interpretations regarding the choice of mean curves. Agreement with experiment has been sought on the basis of calculated R_θ and sometimes only achieved through the use of specially chosen initial H values.

---

* In Fig. 5 of Maskell's paper, the favourable pressure-gradient H values for the same R_θ values (as quoted from Schubauer and Klebanoff) lie above the flat plate results. This discrepancy is removed if the recalculated H values of this investigation are used.

4.5.3. *The equations of Spence and Norbury.*—A thorough evaluation of Spence's auxiliary equations is of some practical importance, as they have been used in recent methods of calculating shape-factor development in three-dimensional layers (Cooke[11]) and for the two-dimensional layer with distributed suction (Dodds[12]). The final form of Spence's auxiliary equation (Spence[61]), used in the present calculations, has already been shown to give generally poor agreement with experiment, Figs. 14 to 24. The earlier versions (Spence[58, 60]) have however been used exclusively in all Spence's published calculations, and have also been used by Norbury[39] to obtain an equation applicable to the boundary layer in the plane of symmetry of a three-dimensional diffuser flow.

(a) *The earlier equation of Spence*[60].

From the equation of motion at $y = \theta$, where the universal logarithmic inner law is assumed to be valid, and the momentum integral equation (7), Spence obtains

$$\gamma \frac{d\gamma}{dx} - \frac{A\gamma}{\theta}\left(\frac{U_\tau}{U_1}\right)^3 = \frac{1}{U_1}\frac{dU_1}{dx}\left[1 - (H+2)A\frac{U_\tau}{U_1}\gamma - \gamma^2\right] + \left[\frac{\partial \dfrac{\tau}{\rho U_1^2}}{\partial y}\right]_{y=\theta} \tag{29}$$

where the shape-factor

$$\gamma = \left(\frac{u}{U_1}\right)_{y=\theta} = \left[\frac{H-1}{H(H+1)}\right]^{\frac{H-1}{2}}$$

from the power-law profiles $u/U_1 = (y/\delta)^{(H-1)/2}$. In addition, $A = 2{\cdot}5$ from the assumed inner law

$$\frac{u}{U_\tau} = 2{\cdot}5 \log_e \frac{U_\tau y}{\nu} + 5{\cdot}5\,.$$

Spence then assumes

$$(H+2)A\frac{U_\tau}{U_1} = 2k_s\,,$$

and

$$\left[\frac{\partial \dfrac{\tau}{\rho U_1^2}}{\partial y}\right]_{y=\theta} = -\alpha_s(1-2k_s\gamma-\gamma^2)\frac{1}{U_1}\frac{dU_1}{dx}\,,$$

where α_s, k_s are free constants, found from the experiments of Gruschwitz, von Doenhoff and Tetervin, and Schubauer and Klebanoff, to be $\alpha_s = -0{\cdot}18, \quad k_s = 0{\cdot}2$.

Now, for $\gamma < 0{\cdot}82$ (*i.e.* $H > 1{\cdot}1$ approx.), these values give $\epsilon < 0$,
where

$$\epsilon = \frac{\left[\dfrac{\partial \dfrac{\tau}{\rho U_1^2}}{\partial y}\right]_{y=\theta}}{\left[-\dfrac{1}{U_1}\dfrac{dU_1}{\partial x}\right]} = \frac{\left[\dfrac{\partial \dfrac{\tau}{\rho U_1^2}}{\partial y}\right]_{y=\theta}}{\left[\dfrac{\partial \dfrac{\tau}{\rho U_1^2}}{\partial y}\right]_{y=\theta}} = \alpha_s(1-2k_s\gamma-\gamma^2)\,. \tag{30}$$

The direct measurements of Newman[37], and Schubauer and Klebanoff[53], show however that $\epsilon > 0$ in moderate or strong adverse pressure gradients, and as Norbury has pointed out, in small pressure gradients ϵ is large, becoming infinite in zero pressure gradient. Thus no choice of constant α_s, k_s is justifiable if the equation is to be useful in practical conditions.

Two main criticisms may be made:

(1) The assumptions for k_s, α_s appear to have been dictated by mathematical convenience as then the auxiliary equation (29) could be reduced to a quadrature form. Thus the physical plausibility of the original approach was lost and the resulting equation can only be regarded as empirical in nature, with the assumptions for overall profile shape introducing further errors.

(2) This equation cannot be considered adequately substantiated on the basis of only two comparisons with measured boundary-layer development as shown originally, where agreement with experiment was obtained by the use of special starting conditions. For Schubauer and Klebanoff, only the adverse pressure-gradient region was calculated, Fig. 21, thus avoiding the difficulties encountered in nearly zero pressure gradients. The starting value of $H_i = 1{\cdot}43$ used to obtain overall agreement with von Doenhoff and Tetervin's aerofoil boundary layer is not justified for the forced transition used, and other methods obtain comparable agreement without needing special H_i assumptions.

(b) *Norbury's modifications.*

Norbury put $2k\gamma = \epsilon + A(H+2).\dfrac{U_\tau}{U_1}\gamma$ in equation (29) and found

$$k = k(H_i{}^3\Gamma, R_\theta),$$

from the experiments used by Spence, and the data of McCullough and Gault[36], Altman and Hayter[1], and his own diffuser measurements.

This allowed empirically for the variation of ϵ over a wide range of H, R_θ, and Γ_1, but whilst non-lifting aerofoils and diffuser data correlated well, he could not relate lifting aerofoil results properly.

Norbury compared his new equation with experiment on the basis of measured R_θ, obtaining better results than Spence in at least one example, and in another his result is close to that of Maskell.

He extended his method to three-dimensional flow, the calculation for the development along the plane of symmetry now making use of a correlation for the change in k (from its corresponding two-dimensional value) in terms of θ/X, where $X(= x+x_0$ in Kehl's notation) is the distance from the source of the local effective radial flow, defined by the intersection of tangents to the external streamlines and the centreline.

Norbury's correlations are difficult to explain in physical terms and his definition of H_i is not altogether clear, but this work must be recognised as one of the few cases where an auxiliary equation has been developed to account explicitly for cross-flow effects.

(c) *The final form of Spence's auxiliary equation* (*Spence*[61]).

The method of derivation of this equation can be shown to account for the excessive sensitivity of calculated H to changes in pressure distribution and in initial H value.

Spence introduced the generalised auxiliary equation (18) via a shear-stress analysis and then derived a simple auxiliary equation by considering a convenient analytic approximation to the P curves of Maskell, Schuh[55] and his own earlier equation. This he justified for the special case of thick boundary layers where,

$$\theta\frac{dH}{dx} = P\,.\,\Gamma_1 = \Phi\,(H)\,.\left[-\frac{\theta}{U_1}\frac{dU_1}{dx}\right], \tag{31}$$

i.e.

$$\frac{dH}{\Phi(H)} = -d(\log_e U_1). \tag{32}$$

He shows curves of H *vs.* $\log_e \frac{U_1}{U_{1i}}$, for $H_i = 1{\cdot}4$.

Agreement between these three functions is quite good, as claimed by Spence, and they only differ by approximately $\pm$ 4 per cent in terms of predicted pressure recovery, for a given H value, although percentage differences in H are very much greater than this for a given U_1/U_{1i}.

For the coefficient Q in this new equation, he used the similarity analysis of Coles[7] for wholly zero pressure-gradient conditions. This yields an analytic expression based upon the universal velocity profile that Coles assumed and the corresponding flat-plate skin-friction law. This expression was incorrectly assumed to hold for the range of H values ($H > 1{\cdot}5$, approximately) for which, in practice, a fully turbulent zero pressure-gradient layer cannot be obtained on smooth walls. This results in Q being much smaller than the values used by other investigators (except for Rubert and Persh, and Schuh) for $H > 1{\cdot}5$, thus providing little restraint on dH/dx, as described in Section 4.4. Even within the range of H values that can be obtained in a real flat-plate turbulent layer, the use of the equilibrium result regardless of upstream conditions ignores the real variation of Q with R_θ, for a given H value, as the equilibrium analysis assumes that H and R_θ are uniquely related {that is $H = H_0(R_\theta$, only)}.

Q should be found (in principle) by the extrapolation of experimentally determined curves of $\theta\, dH/dx$ *vs.* Γ_1, to $\Gamma_1 = 0$, for suitable combinations of H and R_θ. If it is desired to simplify the auxiliary equation by ignoring the effects of R_θ, then the average value of Q, over a sufficient range of R_θ for which fully turbulent flow is possible, should be taken. This has been done by Maskell[35], and others, and usually leads to better shape-factor predictions than are obtained from Spence's equation, as shown by the comparisons already discussed in Section 4.4.

This later form of Spence's equation is slightly poorer than his earlier (published) equation, as shown in Fig. 21, where the two forms are compared on the basis of a full calculation using the two-dimensional momentum equation (7).

(d) *Conclusions.*

This approach is less satisfactory than some of the earlier attempts to calculate the shape-factor development in the same experimental boundary layers and it is unduly sensitive to the choice of initial H value.

The physical realism of the basic assumptions has been lost in an effort to obtain mathematical simplicity and the equation has not been adequately substantiated by direct comparison with a wide range of experimental data.

In fairness, however, it should be pointed out that Spence's method was primarily intended for calculations in adverse pressure gradients leading to separation so that its shortcomings in zero or favourable pressure gradients may not be regarded too seriously. Nevertheless, it is important that the limitations of the method should be recognised, in view of its use as a basis for some newer calculation procedures and its prominent place in recent review articles (*e.g.* Thwaites[67], Duncan, Thom and Young[15]).

4.5.4. *The use of the energy equation—the methods of Rotta, Truckenbrodt, Rubert and Persh, Schuh, Tani, Kawasaki and Walz.*—The second member of the infinite series of integral

relationships is important because of its physical interpretation as an equation for the energy balance in the turbulent boundary layer.

It may be written

$$\frac{1}{2}\frac{d}{dx}(U_1^3\epsilon) = \int_0^\infty \frac{\tau}{\rho}\frac{\partial u}{\partial y}\,dy + \left[\int_0^\infty u\frac{\partial}{\partial x}(\overline{u'^2}-\overline{v'^2})\,dy\right]. \tag{6}$$

The normal-stress term is always (formally) neglected, although (with the exception of a semi-empirical check by Rubert and Persh using the data of Schubauer and Klebanoff) no direct test of this appears to have been made. The measurements of Newman[37], and Sandborn and Slogar[48] are now available and would provide further information for layers approaching separation, where this assumption might be unsatisfactory.

(a) *Basic equations.*

A clearer physical understanding is obtained by considering the equations for mean-flow and turbulence kinetic energy separately, following Rotta[45, 46], Townsend[68] and others.

The equation for mean flow kinetic energy is obtained by multiplying equation (1) by u,

$$\frac{1}{2}u\frac{\partial u^2}{\partial x} + \frac{1}{2}v\frac{\partial u^2}{\partial y} - \frac{1}{2}u\frac{dU_1^2}{dx} - (\overline{u'^2}-\overline{v'^2})\frac{\partial u}{\partial x} - \overline{u'v'}\frac{\partial u}{\partial y} +$$

Loss of mean flow K.E. Turbulence K.E. production.

$$+\frac{\partial}{\partial x}\left[u(\overline{u'^2}-\overline{v'^2})\right] + \frac{\partial}{\partial y}\left[u\overline{(u'v')}\right] - \frac{\nu}{2}\frac{\partial^2 u^2}{\partial y^2} + \nu\left(\frac{\partial u}{\partial y}\right)^2 = 0 \tag{33}$$

Turbulent transfer of mean flow K.E. Viscous transfer Viscous dissipation.

Manipulation of the Navier-Stokes equations with the introduction of the continuity equation gives the turbulence kinetic energy balance,

$$\frac{1}{2}u\frac{\partial\overline{q'^2}}{\partial x} + \frac{1}{2}v\frac{\partial\overline{q'^2}}{\partial y} + (\overline{u'^2}-\overline{v'^2})\frac{\partial u}{\partial y} + \overline{u'v'}\frac{\partial u}{\partial y} + \frac{\partial}{\partial y}\left(\frac{1}{2}\overline{q'^2v'} + \frac{\overline{p'v'}}{\rho}\right) +$$

Convective loss Production Turbulent diffusion

$$+ d - \nu\frac{\partial^2}{\partial y^2}\left(\frac{1}{2}\overline{q'^2} + \overline{v'^2}\right) = 0. \tag{34}$$

Viscous dissipation of turbulence K.E. Viscous diffusion

Combining (33) and (34)

$$\frac{1}{2}\left[u\frac{\partial}{\partial x}(u^2+\overline{q'^2})+v\frac{\partial}{\partial y}(u^2+\overline{q'^2})-u\frac{dU_1^2}{dx}\right]+\frac{\partial}{\partial x}u(\overline{u'^2}-\overline{v'^2})+$$

Loss of total K.E. — Longitudinal transfer by turbulent normal stresses.

$$+\frac{\partial}{\partial y}\left[u(\overline{u'v'})+\frac{1}{2}\overline{v'q'^2}+\overline{\frac{v'p'}{\rho}}\right]-\nu\frac{\partial^2}{\partial y^2}\left[\frac{1}{2}u^2+\frac{1}{2}\overline{q'^2}+\overline{v'^2}\right]+$$

Lateral diffusion terms

$$+D=0, \tag{35}$$

Total viscous dissipation

where

$$D=\nu\left(\frac{\partial u}{\partial y}\right)^2+d. \tag{36}$$

Integrating (35) gives the following alternative version of (6):

$$\frac{1}{2}\frac{dU_1^3\epsilon}{dx}-\frac{1}{2}\frac{d}{dx}\int_0^\infty u\overline{q'^2}\,dy=\int_0^\infty D\,dy+\frac{\partial}{\partial x}\int_0^\infty u(\overline{u'^2}-\overline{v'^2})\,dy \tag{37}$$

Integrating (34) and using (36), or combining (37) and (6), we obtain

$$\int_0^\infty D\,dy=\int_0^\infty\frac{\tau}{\rho}\frac{\partial u}{\partial y}\,dy-\int_0^\infty(\overline{u'^2}-\overline{v'^2})\frac{\partial u}{\partial x}\,dy-\frac{1}{2}\frac{d}{dx}\int_0^\infty u\overline{q'^2}dy. \tag{38}$$

This relates the dissipation integral to the shear work integral, and as recognised by Rotta, the mean-flow energy which has been converted to turbulence energy need not be dissipated by viscosity at the same location. In a rapidly developing layer the rate of change of flux of turbulence kinetic energy cannot be neglected. In the literature (Kawasaki, Rubert and Persh, etc.) confusion is caused by using the name 'dissipation integral' for the shear work integral without any qualification.

In practice, although the term 'dissipation integral' is used, equation (6) is taken as the basis of the auxiliary equation, the main problem being that of determining a suitable relationship for the shear work integral. However, Rotta[45] has endeavoured to separate out the dissipation integral and his expressions have been used by Truckenbrodt[71].

In view of the widespread use of Truckenbrodt's method, especially in Germany (*e.g.* Schlichting[50], Pechau[41]) it has been used in the present series of calculations.

(b) *The derivation of the basic auxiliary equation.*

Equation (6) is expanded and $d\theta/dx$ is eliminated by using equation (5). Thus

$$\theta\frac{dH_e}{dx}=(H+1)H_e\frac{\theta}{U_1}\frac{dU_1}{dx}-\frac{c_f}{2}H_e+e, \tag{39}$$

where

$$e=\left[2\int_0^\infty\frac{\tau}{\rho U_1^2}\frac{\partial\frac{u}{U_1}}{\partial y}\,dy+\frac{2}{U_1^2}\int_0^\infty\frac{u}{U_1}\frac{\partial}{\partial x}(\overline{u'^2}-\overline{v'^2})\,dy-\frac{H_e}{U_1^2}\frac{d}{dx}\int_0^\infty(\overline{u'^2}-\overline{v'^2})\,dy\right] \tag{40}$$

This equation is then normally used, with the assumption of two-dimensional flow, to determine e from experiment. The normal-stress terms are assumed to be negligible and this provides an empirical correlation for the work integral. A velocity-profile family may be used to relate H and H_e but it is generally preferable to find dH_e/dx directly from experiment rather than convert equation (39) to a form involving dH/dx explicitly, as errors in calculated dH_e/dH may be quite large. For the same reason it is better to use (39) as an auxiliary equation for $H_e(x)$, finding $H(x)$ afterwards, if required.

The provision of the above correlations and a suitable skin-friction law completes the development of the auxiliary equation, different forms arising according to the different assumptions made.

(c) *Different forms of the auxiliary equation.*

Rubert and Persh[47] used the shape-factor relationship $H_e = 4H/(3H-1)$, corresponding to the power-law profile family $\frac{u}{U_1} = \left(\frac{y}{\delta}\right)^{(H-1)/2}$, together with the Ludwieg and Tillmann skin-friction law, to bring (39) into the form

$$\theta \frac{dH}{dx} = -\left[H(3H-1)(H-1)\right] \frac{\theta}{U_1} \frac{dU_1}{dx} + \left[\frac{c_{fLT}}{2} H(3H-1)\right] - \frac{(3H-1)^2}{4} e. \tag{41}$$

From (41) and experimental values of $\theta\, dH/dx$, H, R_θ, and $\frac{\theta}{U_1}\frac{dU_1}{dx}$ they found an analytic expression for e. In functional terms this could be written as,

$$e = [f_1(H) + f_2(H) \,.\, \Gamma_1]\, c_{fLT}. \tag{42}$$

Their final correlations were limited to the range

$$1{\cdot}286 \leqslant H \leqslant 2{\cdot}0; \qquad 0 \leqslant \Gamma_1 \leqslant 0{\cdot}004,$$

and required linear extrapolation with respect to Γ_1 for use in the present calculations, this procedure being suggested by the original authors. Scatter of $\pm$ 10 per cent is recorded in Fig. 7 of the original paper, due in part to graphical differentiation.

The poor results given by this equation are due to the very small value of Q, which may result from the absence of the direct use of zero-pressure gradient data, or more probably from the over-simplified analytic form chosen for the correlations at low values of Γ_1. The predominantly convergent flow data of Mangler[34], Weighardt, von Doenhoff and Tetervin, Schubauer and Klebanoff ($x > 17$ ft) were employed and the unusual behaviour of the P curve at low Reynolds numbers ($R_\theta \approx 10^3$), as seen in Fig. 27, results from the matching of such experiments, as the fall of H in adverse pressure gradients could not otherwise be predicted with such very small values of Q.

Following the semi-empirical analysis of the measurements of Weighardt, Tillmann, Ludwieg and Tillmann, and Schultz-Grunow by Rotta[45], Truckenbrodt[71] found a suitable expression for the work integral, which enabled him to reduce (39) to a directly integrable form.

Thus, by choosing the mean line, Fig. 30, to Rotta's curves, he obtained

$$e = \frac{2\beta(H)}{R_\theta{}^p}, \qquad \text{where} \qquad p = \frac{1}{6}; \qquad \beta = 0{\cdot}0056. \tag{43}$$

Rotta used a two-parameter profile family based upon a linear deviation in the outer region from an assumed universal inner law; a single-parameter approximation was however used by Truckenbrodt and may lead to errors in the region of $\pm$ 20 per cent in dU_e/dH for $R_\theta > 10^3$.

The skin-friction law was approximated by

$$c_f = \frac{\alpha(H)}{R_\theta{}^q}, \qquad \text{where} \qquad q = \frac{1}{6}; \qquad \alpha = 0{\cdot}0065. \tag{44}$$

Combining (39), (43) and (44) gives

$$\theta \frac{dH_e}{dx} = (H-1)H_e \frac{\theta}{U_1}\frac{dU_1}{dx} + R_\theta{}^{-p}\left[2\beta - \frac{\alpha(H)\,.\,H_e}{2R_\theta{}^{q-p}}\right].$$

Hence

$$\theta R_\theta{}^p \frac{dH_e}{dx} = F(H_e)\left[\frac{\theta R_\theta{}^p}{U_1}\frac{dU_1}{dx}\right] + G(H_e, R_\theta). \tag{45}$$

Introducing

$$L(H_e) = \int \frac{dH_e}{F(H_e)} = L(H),$$

and

$$K(L, R_\theta) = -\frac{G}{F},$$

this becomes,

$$\frac{dL}{dx} + \frac{K(L, R_\theta)}{\theta R_\theta{}^p} = \frac{1}{U_1}\frac{dU_1}{dx}. \tag{46}$$

Approximating for K, as in Fig. 31 if $R_\theta(x)$ is known from a separate quadrature or from experiment (46) becomes

$$L = L_i \frac{\xi_i}{\xi} + \log_e \frac{U_1}{U_i} + \frac{1}{\xi}\int_{\xi_i}^{\xi}\left[b(R_\theta) - \log_e \frac{U_1}{U_i}\right] d\xi, \tag{47}$$

where $K = a[L - b(R_\theta)]$; $a = 0{\cdot}034$, $b(R_\theta) = 0{\cdot}07 \log_{10} R_\theta - 0{\cdot}23$, and the integrating factor is $\xi = \exp \int \frac{1}{\theta R_\theta{}^p}\, dx$.

$K(L, R_\theta)$ depends upon the difference of the expressions for the work integral and the skin friction and could be considerably in error at larger H values due to the approximations (43) and (44) used by Truckenbrodt.

It seems clear, however, that even if the above manipulation is permissible for most practical purposes, and if Rotta's original analysis is an accurate summary of a sufficient selection of data, then the further drastic linear approximation adopted for K will lead to a systematic over-estimation of dH/dx in adverse pressure gradients (except for the conditions represented in Fig. 31 by the shaded areas; for example $H > 1{\cdot}8$ at $R_\theta = 10^4$) as has already been seen in the present calculations, Figs. 16 and 17, although quite good results may be expected for lower R_θ values as shown in the single example given by Truckenbrodt.

Walz[72] did not seek a simple mathematical form, and used the original K curves shown by Truckenbrodt, without any approximation. He used an extrapolated version of Ludwieg and Tillmann's law giving better values of skin friction for $H > 2{\cdot}0$, and retained a single curve for the shape-factor relationship, using the form adopted by Rubert and Persh, which is rather different from Rotta's curves. The P, Q curves (not shown here) for this equation indicate that improved results are likely for

$$R_\theta \geqslant 10^4 \qquad \text{and} \qquad H < 1{\cdot}7.$$

The evaluation of experimental data, carried out by Rotta to determine the expression for e used as a basis for the above equations, contains two interesting features:

(i) He used hot-wire measurements of $\overline{u'^2}/U_\tau^2$ obtained by Tillmann to suggest the possibility of a single-parameter family of distributions of turbulence energy $\overline{q'^2}/U_\tau^2$. From this he tentatively proposed that the variation of the flux of turbulence energy made little contribution to (38) and hence the usual neglect of the normal stress terms leads to the determination of the true dissipation integral in two-dimensional flow as

$$e = \frac{2}{U_1^3}\int_0^\infty D\,dy. \tag{48}$$

(ii) He determined the dissipation integral from imperfectly two-dimensional boundary layers using a first order allowance for cross-flow based on Kehl's momentum equation,

$$\frac{d\theta}{dx} + \frac{\theta}{(x+x_0)} = \frac{c_f}{2} - (H+2)\frac{\theta}{U_1}\frac{dU_1}{dx}. \tag{24}$$

Local values of $(x+x_0)$ were calculated from the difference between two-dimensional and experimental $d\theta/dx$ values, and were inserted in the corresponding form of the energy equation,

$$\frac{1}{2}\frac{dU_1^3\epsilon}{dx} + \frac{1}{2}\frac{U_1^3\epsilon}{(x+x_0)} = \int_0^\infty D\,dy + \left[\frac{d}{dx}\int_0^\infty u\overline{q'^2}\,dy + \frac{\int_0^\infty \overline{uq'^2}dy}{(x+x_0)}\right]. \tag{49}$$

In spite of the care taken in this derivation there is considerable scatter, Fig. 32, about the mean curve proposed originally by Rotta (and believed to be the basis of the curves shown in Fig. 30), especially for lower H, R_θ conditions.

This makes the accuracy of the expression (43) for e used by Truckenbrodt, and Walz, subject to several uncertainties especially as an allowance for three-dimensional effects is made in its derivation but not included when it is used in a calculation and compared to imperfectly two-dimensional experiments. However, it represents the first proper attempt to separate out the influence of cross-flow and to obtain correlations which should lead to improved results in closely two-dimensional circumstances.

The following investigators have obtained alternative expressions for e:

Schuh[55] made similar assumptions to Rubert and Persh, but put $e = a(H) + b(H).\ \Gamma_1$, and obtained,

$$\theta\frac{dH}{dx} = c(H) + d(H)\,.\,\Gamma_1, \tag{50}$$

where $c(H)$, $d(H)$ were found from experiment.

Tani[65] used similarity solutions to derive e from (39), $\frac{dH}{dx}$ being approximately zero in this case, so that

$$e = h_1(H, R_\theta) + h_2(H, R_\theta)\,.\,\Gamma_1. \tag{51}$$

Kawasaki[29] repeated the similarity analysis using the two-parameter velocity-profile family of Coles[8] and the associated skin-friction law. He realised that the pressure gradient is matched to the profile properties in an equilibrium layer, and that the relationship (51) should be written

$$e = h_1(H, R_\theta) + h_2(H, R_\theta)[\Gamma_1]_E, \tag{52}$$

where $[\Gamma_1]_E (= f(H, R_\theta))$ is a form parameter, and the use of (52) in non-equilibrium conditions requires that

$$e = e(H, R_\theta) \text{ only}. \tag{53}$$

(d) *Discussion.*

The most general relationship proposed for the work integral is of the form,

$$e = f_1(H, R_\theta) + f_2(H, R_\theta) \,.\, \Gamma_1. \tag{54}$$

Now, even if the local Reynolds stress distribution can be specified adequately by the parameters H, R_θ and Γ_1, this linear function of Γ_1 may be unduly restrictive. It is more likely, however, that the stresses depend also upon the upstream development of the layer although no means of relating e to other than purely local quantities is known at the present time.

The main advantage of considering the dissipation integral separately could be claimed to be that nearly all the dissipation occurs in the region of local similarity close to the wall. However, this is unlikely to be a good assumption in conditions of strongly rising pressure although direct measurements of the energy balance, including any three-dimensional effects, are difficult and consequently no direct information is available concerning the dissipation or work integral under these conditions.

4.5.5. *The entrainment equation.*—Head[25] considered the rate of growth of the quantity flow in the boundary layer. On the basis of a simple dimensional argument he derived a physically plausible auxiliary equation which, in principle, may be extended to more complex situations and is therefore worth careful consideration. The present series of calculations show this to be the best equation so far encountered in the literature.

The quantity flow in the boundary layer (Q) is given by

$$Q = \int_0^\delta u \, dy = U_1(\delta - \delta^*), \tag{55}$$

where Head arbitrarily chose $\delta = (y)_{u/U_1=0{\cdot}995}$.

Assuming that only the larger scales of the turbulent motion affect the entrainment process, these are specified by scales of velocity (U_1) and of length ($\delta - \delta^*$) {chosen to be consistent with (55)}, and some measure of the distribution of boundary-layer properties. To specify the latter the shape factor $H_1 = H_{\delta-\delta^*} \left(= \dfrac{\delta - \delta^*}{\theta} \right)$ was chosen.

Thus $v_e = f(H_1, \delta - \delta^*, U_1)$, where the entrainment velocity $v_e = \dfrac{dQ}{dx} = \dfrac{d}{dx}[U_1(\delta - \delta^*)]$. Dimensional analysis then gives the result

$$\frac{v_e}{U_1} = \frac{1}{U_1}\frac{d}{dx}[U_1(\delta - \delta^*)] = F(H_1). \tag{56}$$

In addition, to relate H and H_1, Head writes

$$H_1 = g(H). \tag{57}$$

Curves representing the functions F and g were obtained from an analysis of the experimental data of Newman[37] and Schubauer and Klebanoff[53]. The curve for F was somewhat arbitrarily chosen since the two sets of data did not agree closely. Difficulties over graphical integration and the definition of δ may mean however that for this very simple approach no more sophistication was

justified. It must be pointed out however that the curve for g appears to take no account of the experimental points for $H < 1{\cdot}4$ and (depending upon R_θ) this may account for the large values of P in the generalised auxiliary equation which lead to the excessive variation of H with pressure gradient already noticed in Figs. 18 and 20.

It should be noticed at this stage that the entrainment process seems unlikely to be seriously influenced by surface conditions (except in so far as they may affect the overall velocity profile) so that the basic correlations for entrainment rate should be suitable for calculations of shape factor development in layers with distributed suction or blowing, equation (56) then taking the form

$$\frac{1}{U_1}\frac{d}{dx}[U_1(\delta-\delta^*) = F(H_1) + \frac{v_0}{U_1}, \tag{58}$$

where v_0 is the transpiration velocity at the surface, with $v_0 > 0$ for injection, and $v_0 < 0$ for suction. In such cases the use of the energy equation would appear to be less satisfactory, as conditions at the wall are likely to influence strongly the overall dissipation and the distribution of shear stress through the layer.

4.6. *Stability of Shape-Factor Calculations.*

It has already been noted that methods vary considerably in their sensitivity to assumed starting values, and this question is now examined in more detail.

There is certainly a sense in which the development of the physical boundary layer itself may be unstable in that small changes in initial conditions may lead to large changes in the subsequent history of the layer. This type of instability was observed experimentally by Clauser[6], and Townsend[70], in his theoretical analysis of equilibrium layers, obtained solutions with small skin friction and large adverse pressure gradients which revealed the existence of two possible boundary layer developments for a given external pressure distribution. It might be expected that any complete calculation method in which the growth of momentum thickness and the development of H were jointly calculated would show the same possibility of divergent behaviour. Here, however, we confine our attention to the stability of the shape-factor calculation when the pressure distribution and the development of momentum thickness are specified.

There is first a somewhat trivial sense in which the shape-factor calculation might be unstable, in that for given initial conditions the course of the step-by-step calculation might be decided by the initial extrapolation from the starting value of $\theta\, dH/dx$, so that the solution does not converge to a unique result. In this sense all the equations examined were stable. In another sense, however, namely in their ability to converge towards a common result for small differences in the starting value of H, all equations showed some measure of instability at sufficiently large values of the pressure gradient parameter Γ_1 although the value of Γ_1 for which divergent behaviour first occurred ($\Gamma_{1\text{crit}}$) varied greatly for different methods.

From the generalised auxiliary equation (21), the rate of divergence of calculated H for given values of R_θ and U_1/ν is

$$\left[\frac{\partial\left(\theta\frac{dH}{dx}\right)}{\partial H}\right]_{\theta,\,\frac{U_1}{\nu}}$$

and the condition for change-over from stable to unstable behaviour is

$$\left[\frac{\partial\left(\theta\frac{dH}{dx}\right)}{\partial H}\right]_{\theta,\frac{U_1}{\nu}} = 0 = \Gamma_{1\text{crit}}\left(\frac{\partial P}{\partial H}\right)_{R_\theta} + \left(\frac{\partial Q}{\partial H}\right)_{R_\theta}$$

Thus,

$$\Gamma_{1\text{crit}} = -\frac{\left(\frac{\partial Q}{\partial H}\right)_{R_\theta}}{\left(\frac{\partial P}{\partial H}\right)_{R_\theta}}. \tag{59}$$

The approximate range of variation of $\Gamma_{1\text{crit}}$ for the equations most frequently considered is shown for $R_\theta = 10^4$ in Fig. 33. The practical significance of the values of $\Gamma_{1\text{crit}}$ may be better appreciated from the following table giving the range of Γ_1 values encountered in some typical experiments.

Newman II	0·001 to 0·0038
Schubauer and Klebanoff	0 to 0·0039 (in the adverse pressure gradient region)
Clauser I	0·0011 approx.
Clauser II	0·002 approx.
Schubauer and Spangenberg 'C'	0·0002 to 0·004
Schubauer and Spangenberg 'D'	0·001 to 0·004
Schubauer and Spangenberg 'E'	0·0005 to 0·00345

Fig. 34 shows the approximate rates of divergence of different equations as given by

$$\left[\frac{\partial\left(\theta\frac{dH}{dx}\right)}{\partial H}\right]_{\theta,\frac{U_1}{\nu}} = \left(\frac{\partial P}{\partial H}\right)_{R_\theta}\Gamma_1 + \left(\frac{\partial Q}{\partial H}\right)_{R_\theta},$$

$$= (1-n)\left(\frac{\partial Q}{\partial H}\right)_{R_\theta},$$

where n is given by

$$\Gamma_1 = n\,\Gamma_{1\text{crit}} \quad i.e. \quad \Gamma_1 = -n\frac{\left(\frac{\partial Q}{\partial H}\right)_{R_\theta}}{\left(\frac{\partial P}{\partial H}\right)_{R_\theta}}.$$

Thus only one value of

$$\left[\frac{\partial\left(\theta\frac{\partial H}{dx}\right)}{\partial H}\right]_{\theta,\frac{U_1}{\nu}}$$

need be found for a suitable value of n, and the reason for the straight line relationships shown in the figure is apparent.

It was not certain, *a priori*, that equations having lower values of $\Gamma_{1\text{crit}}$ would necessarily show less sensitivity to changes in H_i, as regards their overall predictions of $H(x)$, than some equations having higher values. The possibility might exist that a later, more severe, divergence would give an earlier prediction of separation than an earlier, more gradual divergence. However, as Fig. 34 shows for $H = 1{\cdot}8$, $R_\theta = 10^4$ (and this appears to be true for all conditions except for the smallest H values, and for $H = 1{\cdot}5$ in the case of Rubert and Persh) the equations having the lowest values of $\Gamma_{1\text{crit}}$ also exhibit in general the most divergent behaviour.

From Fig. 33 it will be seen that (for $1{\cdot}4 < H < 2{\cdot}2$; $R_\theta = 10^4$) the auxiliary equations in order of increasing $\Gamma_{1\text{crit}}$ are Rubert and Persh; Spence; Truckenbrodt and probably Maskell; Head.

The relative rates of divergence shown in Fig. 34 for $H = 1{\cdot}8$ suggest that the spread of predicted H developments will also be smaller in the order given above. As a check on these conclusions direct calculations were performed for the case of Schubauer and Spangenberg 'D' where $0{\cdot}001 < \Gamma_1 < 0{\cdot}004$. The starting values of H assumed ($H_i = 1{\cdot}40, 1{\cdot}36, 1{\cdot}32$) more than covers the range of experimental uncertainty and may in fact go beyond the condition of small disturbances.

The results of the calculations are shown in Fig. 35 from which it will be seen that the spread of predicted H values is very different for the different methods.

Spence's equation shows a typically rapid divergence as $\Gamma_{1\text{crit}}$ is very small and the rate of divergence large.

$$\Gamma_{1\text{crit}} \approx 0{\cdot}0001 \qquad \text{for} \qquad H > 1{\cdot}4.$$

Truckenbrodt's equation shows only a slow divergence at the large H values.

$$\Gamma_{1\text{crit}} \approx 0{\cdot}0015 \qquad \text{for} \qquad H > 1{\cdot}4.$$

Head's equation shows convergent or neutral stability over the complete range of Γ_1 and H involved, and provides a surprisingly good prediction for the whole of this H development for any of the starting values.

$$\Gamma_{1\text{crit}} \approx 0{\cdot}003 \qquad \text{for} \qquad H > 1{\cdot}4.$$

Whilst this investigation has been restricted to a somewhat artificial situation, in that in practice both H and R_θ would vary downstream of a disturbance, the comparative predictions of different auxiliary equations would be expected to depend only slightly upon the R_θ distribution and it seems reasonable to suppose that the equation yielding the best overall agreement with experiment for plausible values of H_i, $R_\theta(x)$, will contain the greatest measure of physical truth and hence will provide the most reliable estimate of the stability of the real flow. For example, the predictions of Spence, Fig. 35, appear unreasonable and, in many cases, no satisfactory agreement with experiment for any plausible H_i is obtained (due to incompatible P, Q functions) whilst the predictions of Head agree well with experiment and show a convergent behaviour that seems intuitively likely.

The effect of variations in R_θ on calculated H development can be examined, using the generalised auxiliary equation, in a similar way to that which has already been used in discussing the effects of changes in H.

The rate of divergence (sensitivity of H to R_θ) becomes in this case:

$$\left[\frac{\theta\,\partial\left(\frac{dH}{dx}\right)}{\partial R_\theta}\right]_{H,\,\frac{U_1}{\nu}} = \Gamma_1\left(\frac{\partial P}{\partial R_\theta}\right)_H + \left[\left(\frac{\partial Q}{\partial R_\theta}\right)_H - \frac{Q}{R_\theta}\right], \tag{60}$$

and consideration of the expressions for P and Q shows that the equations whose values of Q are small or which vary only slightly with R_θ, such as Spence, Rubert and Persh, and von Doenhoff and Tetervin, will yield predictions for H that are very insensitive to changes in R_θ of the order of the discrepancy between experimental and calculated (two-dimensional) results shown in Figs. 1 to 10. The newer equations such as Head, Truckenbrodt and Maskell appear to be rather more affected by changes in R_θ of this magnitude although, as stated earlier, the relative levels of accuracy of the predictions of these equations are unlikely to be significantly affected. In the two important cases of Clauser I and II (*see* Figs. 36 and 37), this has been confirmed by comparing, for the equations of Spence and Head, the shape-factor predictions obtained on the basis of the momentum growth calculated using two-dimensional theory, in addition to the earlier comparisons using experimental $R_\theta(x)$.

It is suggested that a series of full calculations could be performed solving simultaneously for H and R_θ with a range of values of H_i, $R_{\theta i}$ to investigate the stability of turbulent boundary layers with given external velocity distributions. Clauser I and II are of particular interest in this connection. Furthermore, the effects of large disturbances can easily be considered whereas the mathematical criteria only apply to small disturbances.

Finally, the question also arises as to the stability or otherwise of the strictly two-dimensional state of the time-mean turbulent boundary layer in view of the discovery of quite large quasi-periodic spanwise variations of time-mean quantities in such layers (Head and Rechenberg[26], Fernholz[19]). If (over limited x-distances) there is little interaction between the parts of the layer developing in parallel planes separated by a small z-distance (of the order of the boundary-layer thickness), then calculations using the ordinary approximate methods as suggested above may be carried out for the development in such planes if the spanwise variation of the initial conditions $\{H_i(z); R_{\theta i}(z)\}$ are known or assumed. It may be inferred from the two-dimensional results discussed earlier that these three-dimensional effects will decay except in moderate to large adverse pressure gradients, although the condition of independence at different spanwise position in unlikely to be satisfied for other than small spanwise perturbations.

5. *Conclusions.*

From the examination of experimental data for boundary layers developing in nominally two-dimensional conditions it is concluded that:

(i) the presentation of published data in many cases makes it extremely difficult to abstract accurate experimental values and, in addition, the recalculation of H and R_θ from given profile data which are accurately presented frequently gives values differing significantly from those published,

(ii) the use of a two-parameter profile family and the Clauser plot for the inner law provides a satisfactory criterion for assessing whether the boundary layer is in a fully turbulent condition at the start of a calculation.

Calculations of momentum thickness development, using various forms of the momentum integral equation show that

(iii) the lack of agreement with the two-dimensional momentum integral equation found in nearly all cases is almost certainly due to the presence of three-dimensional effects rather than the inadequacy of assumed skin-friction laws, or the neglect of turbulence terms in the equation,

(iv) empirically modified forms of the momentum integral equation are in no way superior to the unmodified form of the equation in raising the general level of agreement with experiment,

(v) at present, experimental values of R_θ provide the best available basis for comparing measured and calculated H development.

From the comparison of various proposed forms of the auxiliary equation with experiment it is concluded that:

(vi) before any method is accepted for general application it should be checked against the widest possible range of experimental data,

(vii) there is a great need for a limited number of really precise measurements of boundary-layer development either in accurately two-dimensional conditions or in conditions where three-dimensional effects can be accurately assessed,

(viii) the existing equations give widely differing results in many cases, and these results are often inaccurate. Particularly poor results are found for the equilibrium layers of Clauser[6], where H is almost constant. Head's entrainment equation appears to give the best general level of agreement with experiment. The method developed by the present author, but not yet published, is superior in certain cases.

(ix) A generalised auxiliary equation, similar in form to that derived by Spence, summarises concisely the distinctive features of the various equations and gives some insight into the anomalous results given by certain methods.

(x) Examination of the sensitivity of various methods to small changes in starting values shows large differences of behaviour. Head's entrainment equation is shown to be relatively insensitive to starting values while Spence's method gives highly divergent results even in relatively small adverse gradients. Truckenbrodt's method is intermediate in behaviour.

The difficulties inherent in any attempt to predict shape-factor development arise not only because of the absence of a satisfactory knowledge of the relationship between the turbulent (Reynolds) stresses and the mean velocity distribution, but also to the necessity, at the present time, of basing correlations on data obtained in boundary layers which appear to have a three-dimensional flow component but where the measured boundary values are appropriate only to strictly two-dimensional conditions. In a later report it is hoped to publish a method of calculating H development which achieves consistently better results than any of the methods considered in the present paper. This new method is essentially a development of Head's entrainment equation but incorporates fresh physical reasoning and attempts to account explicitly for the effects of any secondary flows that may be present in measured layers.

Acknowledgements.

The author gratefully acknowledges the guidance of Dr. M. R. Head who supervised the above investigation whilst the author was a research student at Cambridge. Thanks are also due to Miss Susan Gray for assistance with the computation.

NOTATION

A, B	Constants in the semi-logarithmic inner law $\left(B = \frac{1}{\kappa}\log_e 10\right)$
c	Aerofoil chord length
c_f	Local value of skin-friction coefficient $\left(= \frac{\tau_0}{\frac{1}{2}\rho U_1^2}\right)$
c_{fLT}	Value of c_f as given by the Ludwieg-Tillmann relationship
d, D	Viscous dissipation terms in the energy equations (34 and 35)
e	Shear work integral, in the energy equation
$H, H_1, H_\epsilon, \overline{H}, H_{\delta-\delta^*}$	Profile shape-factors: $H = \frac{\delta^*}{\theta}$; $H_1 = H_{\delta-\delta^*} = \frac{\delta-\delta^*}{\theta}$; $H_\epsilon = \overline{H} = \frac{\epsilon}{\theta}$.
$H_0 = H_0(R_\theta)$	Denotes the variation of H in a constant pressure boundary layer
P, Q	Functions appearing in the generalised auxiliary equation (21)
Q	Volume flux in the boundary layer
q	Local dynamic pressure in the boundary layer at (x, y); $(= p_0 - p = \frac{1}{2}\rho u^2)$
$\overline{q'^2}$	Turbulence intensity $(= \overline{u'^2} + \overline{v'^2} + \overline{w'^2})$
R	Local radius of curvature of surface (in the x, y plane)
$R_x, R_\theta, R_c,$	Reynolds numbers: $R_x = \frac{U_1 x}{\nu}$; $R_\theta = \frac{U_1\theta}{\nu}$; $R_c = \frac{U_1 c}{\nu}$;
U_1	Component of free-stream velocity vector along the x direction
u, v	Component of the velocity vector in the boundary layer, in the x, y directions respectively
U_1, U_2	Velocity scales used in the order-of-magnitude arguments in the boundary-layer approximation
$\tilde{u}$	Turbulence velocity scale, ditto
u', v'	Instantaneous turbulence velocity components
U_0	Value of U_1, at the reference station $x = x_0$, (not necessarily the same as the initial value U_{1i}, at $x = x_i$)
$\frac{U_1}{\nu}$	Local free-stream Reynolds number per unit length
v_0	Transpiration velocity at the wall (positive for injection)

NOTATION—*continued*

x, y, z	Localised rectangular Cartesian co-ordinates: x is measured along the surface in the longitudinal direction; y is the distance from the surface measured along the local normal direction; z is the spanwise distance
$x + x_0 = X$	The distance measured from the origin of the local effective radial flow
$\Gamma, \Gamma_1, \Gamma_i$	Pressure gradient parameters, $\Gamma = \frac{\theta R_\theta^{1/n}}{U_1}\frac{dU_1}{dx}$; $\Gamma_1 = -\frac{\theta}{U_1}\frac{dU_1}{dx}$
$\Gamma_{1\text{crit}}$	Stability criterion (defined in Section 4·6)
δ^*	Displacement thickness $= \int_0^\infty \left(1 - \frac{u}{U_1}\right) dy$
ΔH	Fall in the value of H at transition (*see* Section 4)
ρ	Density of fluid
τ	Shear stress $\left(= \mu \frac{\partial u}{\partial y} - \rho \overline{u'v'} \right)$
τ_0	Wall shear stress
Φ, Ψ	Functions appearing in the generalised auxiliary equation (18)

Note

Many of the above symbols are used in the review with a different meaning, as attributed to them by the original authors, but no confusion arises as definitions are given in the text.

REFERENCES

No.	Author(s)	Title, etc.
1	J. M. Altman and N. F. Hayter ..	A comparison of the turbulent boundary-layer growth on an unswept and a swept wing. N.A.C.A. TN 2500. September, 1951.
2	W. Bauer	The development of the turbulent boundary layer on steep slopes. Thesis: State Univ. of Iowa—quoted by Coles[8]. 1956.
3	J. M. Bidwell..	Application of the von Karman momentum theorem to turbulent boundary layers. N.A.C.A. TN 2571. December, 1951.
4	P. Bradshaw	Approximate solution of the 'Inverse Problem' of boundary-layer theory. *Jl. R. Aeronaut. Soc.*, Vol. 64, pp. 225–6. 1960.
5	A. Buri	A method of calculation for the turbulent boundary layer with accelerated and retarded basic flow. R.T.P. Translation No. 2073, British Ministry of Aircraft Production, Thesis No. 652, Federal Tech. Coll., Zurich. 1931.
6	F. H. Clauser	Turbulent boundary layers in adverse pressure gradients. *J. Aeronaut. Sci.*, Vol. 21, No. 2, pp. 91–108. 1954.
7	D. Coles	The problem of the turbulent boundary layer. *Z. angew. Math. Phys*, Vol. 5, pp. 181–202. 1954.
8	D. Coles	The law of the wake in the turbulent boundary layer. *J. Fluid Mech.*, Vol. 1, pp. 191–226. 1956.
9	D. Coles	The turbulent boundary layer in a compressible fluid. Report for U.S.A.F. Project Rand. R–403–PR. 1962.
10	J. C. Cooke	A calculation method for three dimensional turbulent boundary layers. A.R.C. R. & M. 3199. October, 1958.
11	J. C. Cooke	Three dimensional turbulent boundary layers. A.R.C. C.P. 635. June, 1961.
12	J. I. Dodds	Ph.D. Dissertation, Cambridge University. 1961.
13	A. E. von Doenhoff and N. Tetervin	Determination of general relations for the behaviour of turbulent boundary layers. N.A.C.A. Report 772. 1943.
14	H. L. Dryden	Some recent contributions to the study of transition and turbulent boundary layers. N.A.C.A. TN 1168. 1947.
15	W. J. Duncan, A. S. Thom and A. D. Young.	*An elementary treatise on the mechanics of fluids.* London: Edward Arnold Ltd. 1960.

No.	*Author(s)*	*Title, etc.*
16	R. A. Dutton	The velocity distribution in a turbulent boundary layer on a flat plate. A.R.C. C.P. 453. October, 1957.
17	A. Fage and W. G. Raymer	Note on empirical relations for a turbulent boundary layer. A.R.C. R. & M. 2255. March, 1946.
18	H. H. Fernholz	Theoretische Untersuchung zur optimalen Druckumsetzung in Unterschall-diffusoren. Dissertation, Karlsruhe. 1961.
19	H. H. Fernholz	Three-dimensional disturbances in a two-dimensional incompressible turbulent boundary layer. A.R.C. R. & M. 3368. October, 1962.
20	H. C. Garner	The development of turbulent boundary layers. A.R.C. R. & M. 2133. June, 1944.
21	F. R. Goldschmied	Skin friction of incompressible turbulent boundary layers under adverse pressure gradients. N.A.C.A. TN 2431. August, 1951.
22	P. S. Granville	A method for the calculation of the turbulent boundary layer in a pressure gradient. David Taylor Model Basin, Rep. 752. May, 1951.
23	E. Gruschwitz	The turbulent layer of friction in two-dimensional flow with pressure drop and increase. Translation of Göttingen Dissertation, 1932.
24	F. R. Hama	Turbulent boundary layer along a flat plate. Rep. Institute Sci. and Tech., Univ. of Tokyo, Vol. 1, pp. 13–16, 49–50. 1947.
25	M. R. Head	Entrainment in the turbulent boundary layer. A.R.C. R. & M. 3152. September, 1958.
26	M. R. Head and I. Rechenberg	The Preston tube as a means of measuring skin friction. *J. Fluid Mech.*, Vol. 14, Pt. 1, pages 1–17. September, 1962.
27	C. T. Hewson	Ph.D. Dissertation, Cambridge University. 1949.
28	J. O. Hinze	*Turbulence; an introduction to its mechanism and theory.* McGraw-Hill. New York. 1959.
29	T. Kawasaki	On an approximate solution of the two-dimensional turbulent boundary layer. *Trans. Japan Soc. aeronaut. Space Sci.*, Vol. 4, No. 5, pp. 1–11. 1961.
30	A. Kehl	Investigations of convergent and divergent turbulent boundary layers. R.T.P. Translation No. 2035, from Ing. Archiv., Vol. 13, No. 5, pp. 293–329. 1943.

No.	*Author(s)*	*Title, etc.*
31	P. S. Klebanoff	Characteristics of turbulence in a boundary layer with zero pressure gradient. N.A.C.A. Report 1247. 1955.
32	P. S. Klebanoff and Z. W. Diehl ..	Some features of artificially thickened fully developed boundary layers with zero pressure gradient. N.A.C.A. Report 1110. 1952.
33	H. Ludwieg and W. Tillmann ..	Investigations of the wall-shearing stress in turbulent boundary layers. N.A.C.A. TM 1285 (1950).
34	W. Mangler	Das Verhalten der Wandschubspannung in turbulenten Reibungsschichten mit Druckanstieg. Aero. Versuchsanst, Gött., UM 3052. 1943.
35	E. C. Maskell	Approximate calculation of the turbulent boundary layer in two-dimensional incompressible flow. R.A.E. Rep. No. Aero. 2443, also A.R.C. 14,654. 1951.
36	G. B. McCullough and D. E. Gault	Examples of three representative types of airfoil-section stall at low speed. N.A.C.A. TN 2502. 1951.
37	B. G. Newman	Some contributions to the study of the turbulent boundary layer near separation. Aust. Dept. Supply Rep. No. ACA–53. 1951.
38	J. Nikuradse	Untersuchungen über die strömungen des Wassers in konvergenten und divergenten Kanälen. Forschungsheft V.D.I. 289—quoted by Ross[44] and others. 1929.
39	J. F. Norbury	An approximate method for the calculation of turbulent boundary layers in diffusers. *Aeronaut Q.*, Vol. 8, pp. 58–77. 1957.
40	J. F. Norbury	Some measurements of boundary-layer growth in a two-dimensional diffuser. *J. Bas. Engng.* (Trans. A.S.M.E. Ser. D), Vol. 81, pp. 285–296. 1959.
41	W. Pechau	Calculation of the turbulent boundary layer with continuously distributed suction. AGARD Rep. 259. 1960.
42	K. Pohlhausen	Zur näherungsweisen Integration der Differentialgleichung der laminaren Grenzschicht. Zeit. ang. Math. Mech., Vol. 1, pp. 252–268. 1921.
43	J. H. Preston	The calculation of lift taking account of the boundary layer. A.R.C. R. & M. 2725. November, 1949.

REFERENCES—*continued*

No.	*Author(s)*	*Title, etc.*
44	D. Ross	A study of incompressible turbulent boundary layers. Ordnance Research Lab. TM ONR Project NR 062–139–1. (Ph.D. Thesis, Harvard University). 1953.
45	J. C. Rotta	On the theory of the turbulent boundary layer. N.A.C.A. TM 1344 (1953).
46	J. C. Rotta	*Turbulent boundary layers in incompressible flow.* *Progress in aeronautical Sciences*, Vol. II, pp. 1–220, Pergamon Press, 1962.
47	K. F. Rubert and J. Persh	A procedure for calculating the development of turbulent boundary layers under the influence of adverse pressure gradients. N.A.C.A. TN 2478. September, 1951.
48	V. A. Sandborn and R. J. Slogar ..	Study of the momentum distribution of turbulent boundary layers in adverse pressure gradients. N.A.C.A. TN 3264. January, 1955.
49	A. J. Sarnecki	Ph.D. Dissertation, Cambridge University. 1959.
50	H. Schlichting	Application of boundary-layer theory in turbomachinery. *J. Bas. Engng.* (Trans. A.S.M.E. Ser. D), Vol. 81, pp. 543–551. 1959.
51	H. Schlichting	*Boundary Layer Theory.* Fourth Edition. New York. McGraw-Hill. 1960.
52	H. Schmidbauer	Turbulente Reibungsschicht an erhaben gekrümmten Flächen. Luftfahrtforschung, Vol. 13, pp. 160–162 (read in a private translation), also N.A.C.A. TM 791. 1936.
53	G. B. Schubauer and P. S. Klebanoff	Investigation of separation of the turbulent boundary layer. N.A.C.A. Report 1030. 1951.
54	G. B. Schubauer and W. G. Spangenberg.	Forced mixing in boundary layers. *J. Fluid Mech.*, Vol. 8, pp. 10–32. 1960.
55	H. Schuh	On calculating incompressible turbulent boundary layers with arbitrary pressure distribution. K.T.H. (Sweden), Aero. Tech. Note No. 41. 1954.
56	G. Schultz-Grunow	New frictional resistance law for smooth plates. N.A.C.A. TM 986. 1941.
57	D. W. Smith and J. H. Walker ..	Skin-friction measurements in incompressible flow. N.A.S.A. TR. R–26. 1958.
58	D. A. Spence..	Ph.D. Dissertation, Cambridge University, pp. 1–35. 1952.
59	D. A. Spence..	Prediction of the characteristics of two-dimensional aerofoils. *J. Aeronaut. Sci.*, Vol. 21, pp. 577–588. 1954.

REFERENCES—*continued*

No.	*Author(s)*	*Title, etc.*
60	D. A. Spence..	The development of turbulent boundary layers. *J. Aeronaut. Sci.*, Vol. 23, pp. 3–15. 1956.
61	D. A. Spence..	Reference to calculation method described in *Incompressible aerodynamics.* Oxford Univ. Press. 1960.
62	H. B. Squire and A. D. Young ..	The calculation of the profile drag of aerofoils. A.R.C. R. & M. 1838. November, 1937.
63	B. S. Stratford	The prediction of separation of the turbulent boundary layer. *J. Fluid Mech.*, Vol. 5, pp. 1–16. 1959.
64	B. S. Stratford	An experimental flow with zero skin friction throughout its region of pressure rise. *J. Fluid Mech.*, Vol. 5, pp. 17–35. 1959.
65	I. Tani	Energy dissipation in turbulent boundary layers. *J. Aeronaut. Sci.*, Vol. 23, pp. 606–607. 1956.
66	N. Tetervin and C. C. Lin	A general integral form of the boundary-layer equation for incompressible flow with an application to the calculation of the separation point of turbulent boundary layers. N.A.C.A. Report 1046. 1951.
67	B. Thwaites	*Incompressible aerodynamics.* Oxford Univ. Press. 1960.
68	A. A. Townsend	*The structure of turbulent shear flow.* Cambridge Univ. Press. 1956.
69	A. A. Townsend	The development of turbulent boundary layers with negligible wall stress. *J. Fluid Mech.*, Vol. 8, pp. 143–155. 1960.
70	A. A. Townsend	Equilibrium layers and wall turbulence. *J. Fluid Mech.*, Vol. 11, pp. 97–120. 1960.
71	E. Truckenbrodt	A method of quadrature for calculation of the laminar and turbulent boundary layer in the case of plane and rotationally symmetrical flow. N.A.C.A. TM 1379. 1955.
72	A. Walz	Beitrag zur Naherungstheorie kompressibler turbulenter Grenzschichten. DVL Ber. Nr. 84. March, 1959.
73	K. Weighardt and W. Tillmann ..	On the turbulent friction layer for rising pressure. N.A.C.A. TM 1314. 1951.
74	F. X. Wortman	A contribution to the design of laminar profiles for gliders and helicopters. English translation, TIL/T. 4903 (1960) from Zeit. Flug W., Vol. 3, pp. 333–345. 1955.

APPENDIX

The Method of Integration of Velocity Profiles to find θ and δ^*

The measured values of $\frac{u}{U_1}, \frac{u}{U_1}\left(1-\frac{u}{U_1}\right)$ were plotted against y on millimetre graph paper to occupy as much of a foolscap page as possible.

The most consistent results were obtained by arranging that the same operator always drew in the mean curve through these measured values and made the extrapolation to the origin. Convenient intervals of y were marked off and the areas of the curves standing on these intervals were found by sliding a piece of celluloid (inscribed with a fine straight line) over the curve until a trapezium of the same area (as under that segment of the curve) was marked off. As the eye is very accurate at comparing small areas between the curve and the inscribed line, this method is quite rapid and accurate and it was preferred to counting squares, to planimetry or to the use of Simpson's rule (even with twice the number of intervals this last method was not always accurate due to the long 'tails' of some of the profiles).

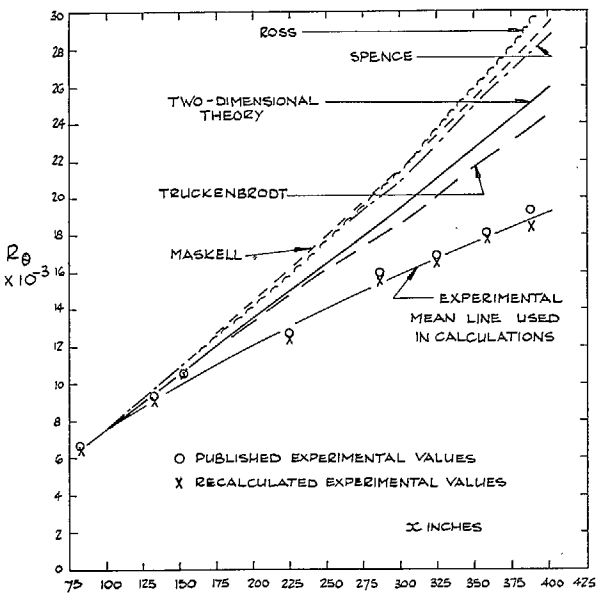

FIG. 1. Clauser (6) Series I.

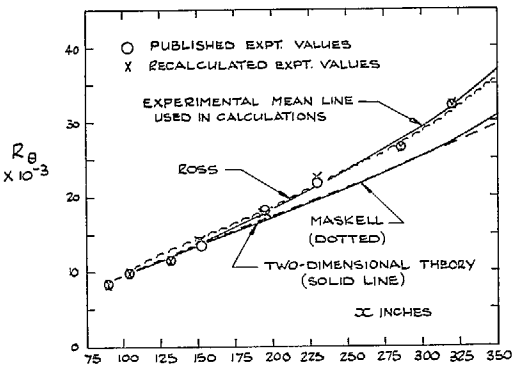

FIG. 2. Clauser (6) Series II.

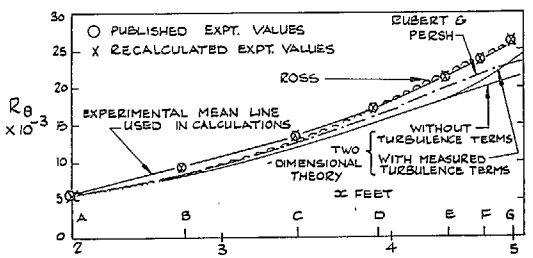

FIG. 3. Newman (37) Series II.

Comparison of calculated momentum developments with experiment.

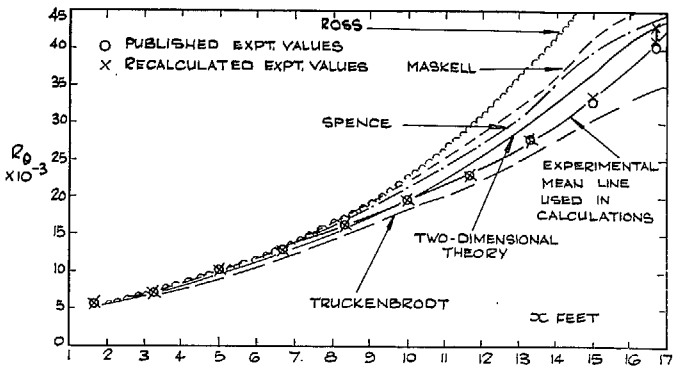

FIG. 4. Schubauer and Spangenberg 'C' (54).

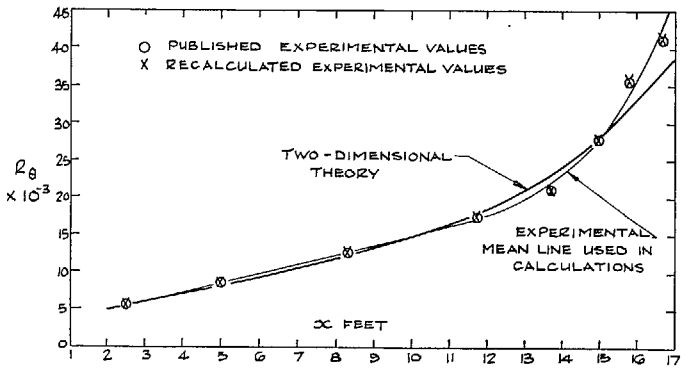

FIG. 6. Schubauer and Spangenberg 'E' (54).

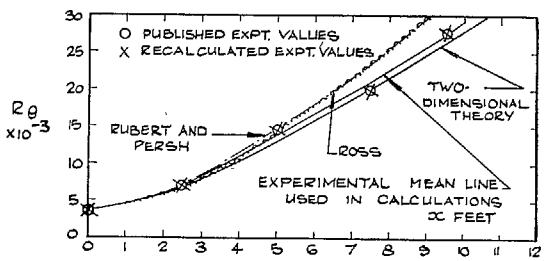

FIG. 5. Schubauer and Spangenberg 'D' (54).

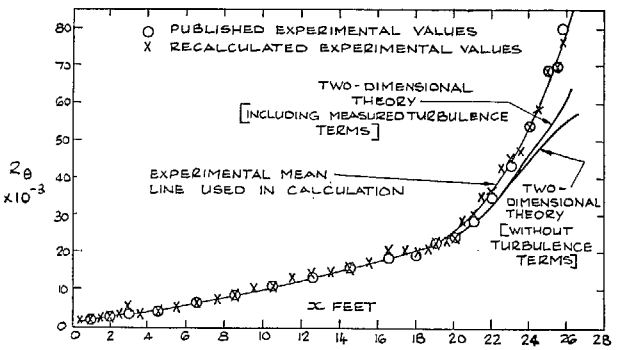

FIG. 7. Schubauer and Klebanoff (53).

Comparison of calculated momentum developments with experiment.

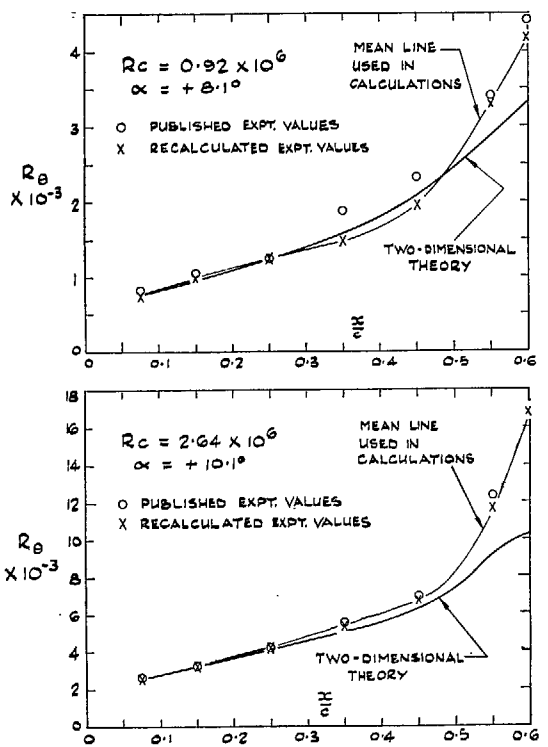

FIG. 8. von Doenhoff and Tetervin (13). [N.A.C.A. 65 (212)–222 aerofoil].

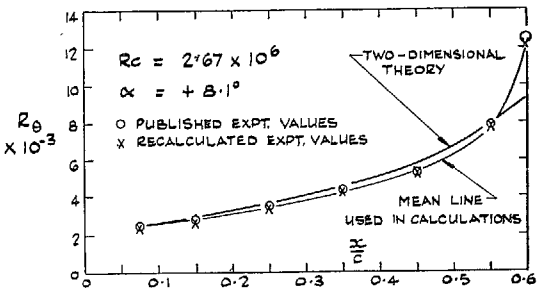

FIG. 9. von Doenhoff and Tetervin (13). [N.A.C.A. 65 (212)–222 aerofoil].

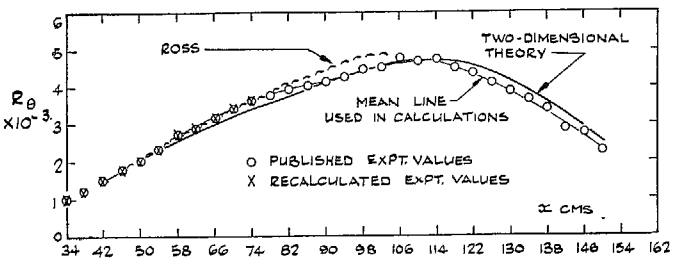

FIG. 10. Schmidbauer (52).

Comparison of calculated momentum developments with experiment.

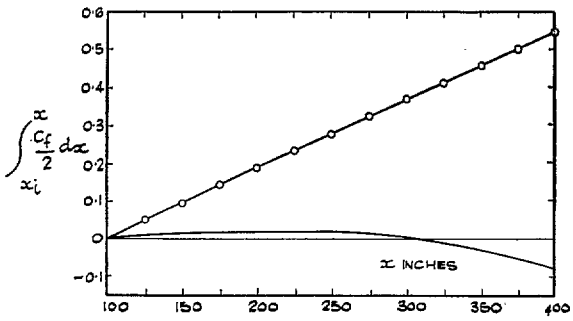

Clauser (6) Series I.

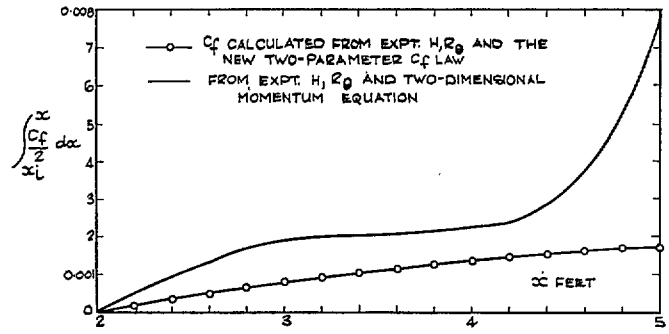

Newman (37) Series II.

FIG. 11. Comparison of skin-friction calculations.

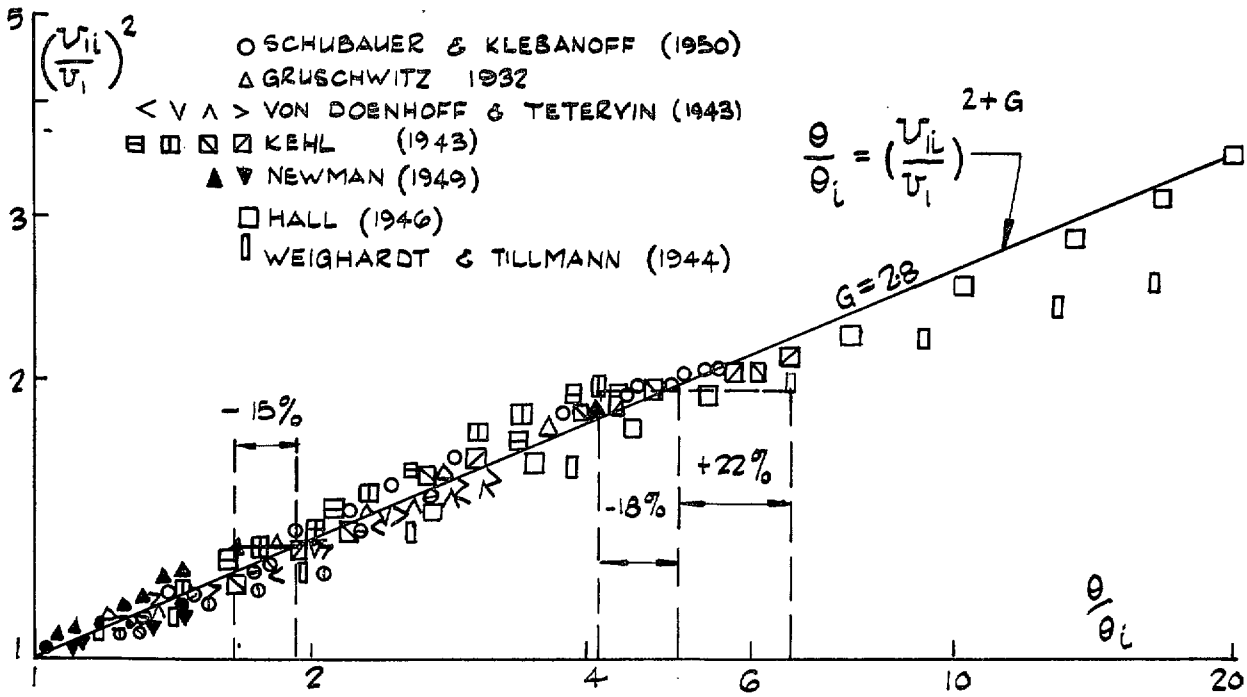

FIG. 12. Momentum thickness relationship proposed by Ross (44) for strong adverse pressure gradient.

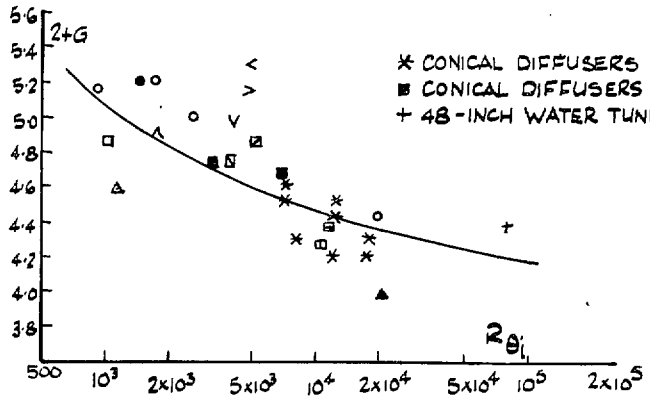

FIG. 13. A further correlation suggested by Ross (44).

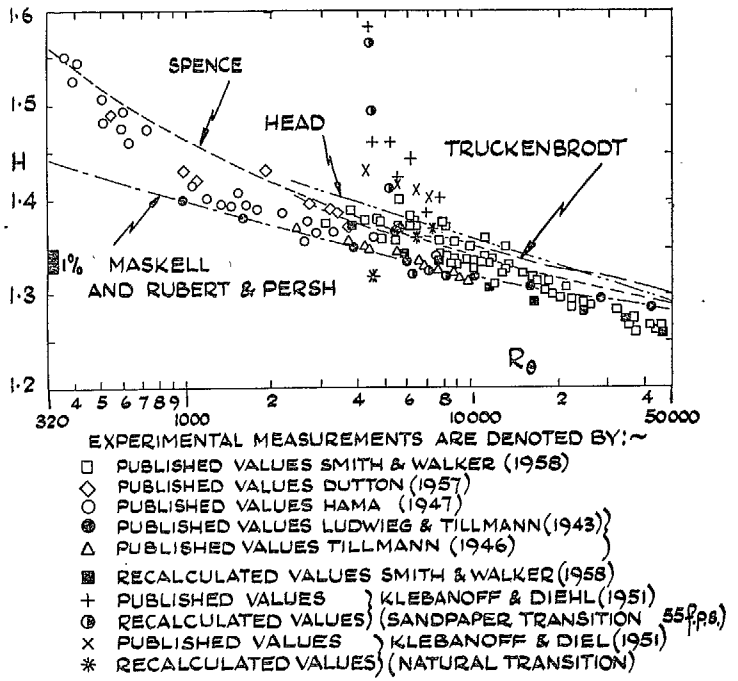

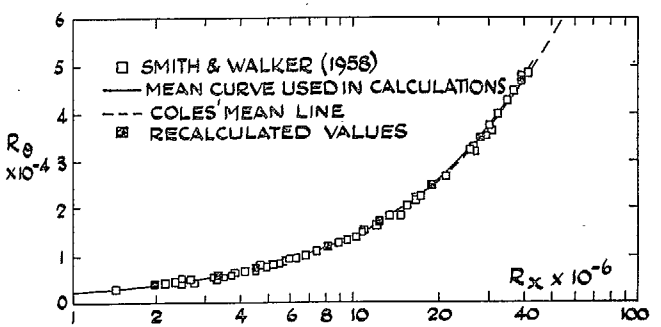

FIG. 14. Shape factor and momentum growth in zero pressure gradient.

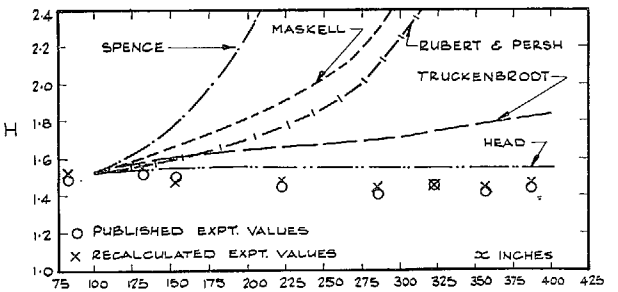

FIG. 15. Clauser (6) Series I.

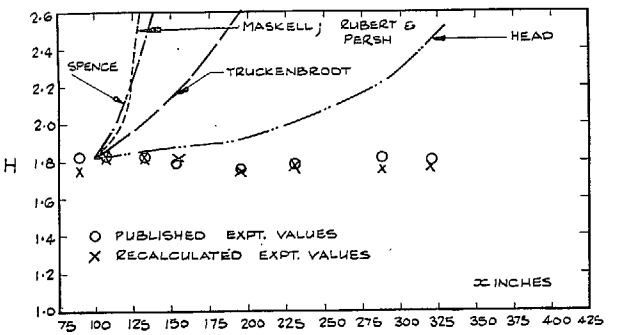

FIG. 16. Clauser (6) Series II.

Comparison of calculated shape-factor developments using different auxiliary equations.

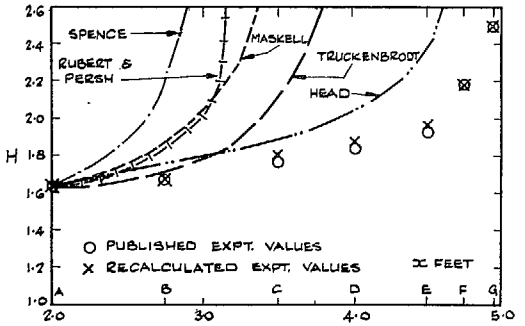

FIG. 17. Newman (37) Series II.

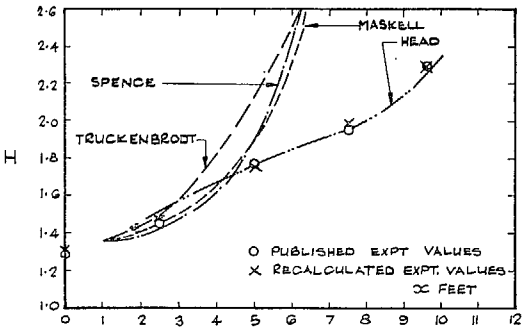

FIG. 19. Schubauer and Spangenberg 'D' (54).

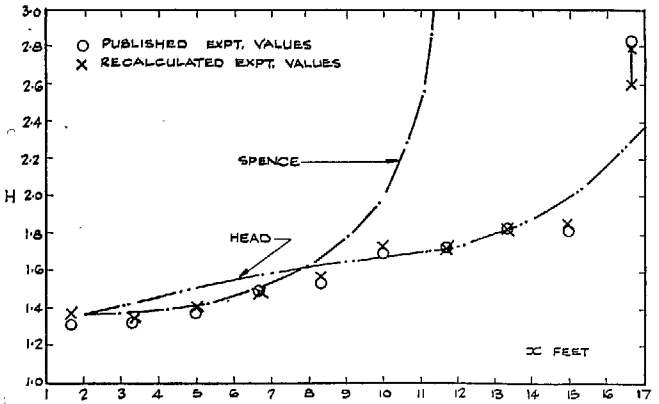

FIG. 18. Schubauer and Spangenberg 'C' (54).

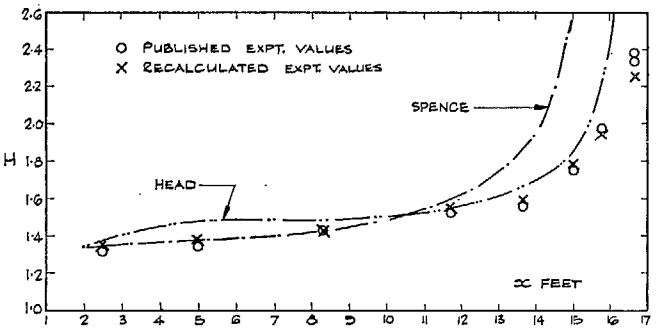

FIG. 20. Schubauer and Spangenberg 'E' (54).

Comparison of calculated shape-factor developments.

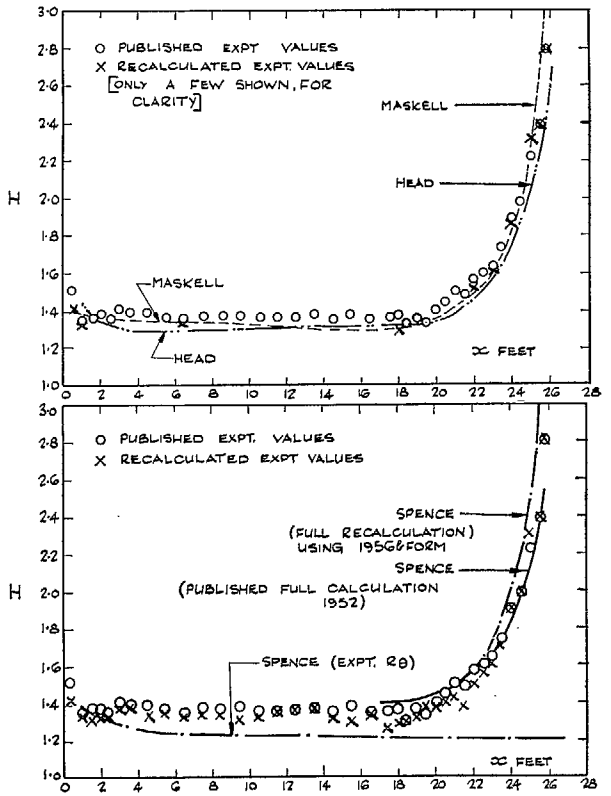

FIG. 21. Schubauer and Klebanoff (53).

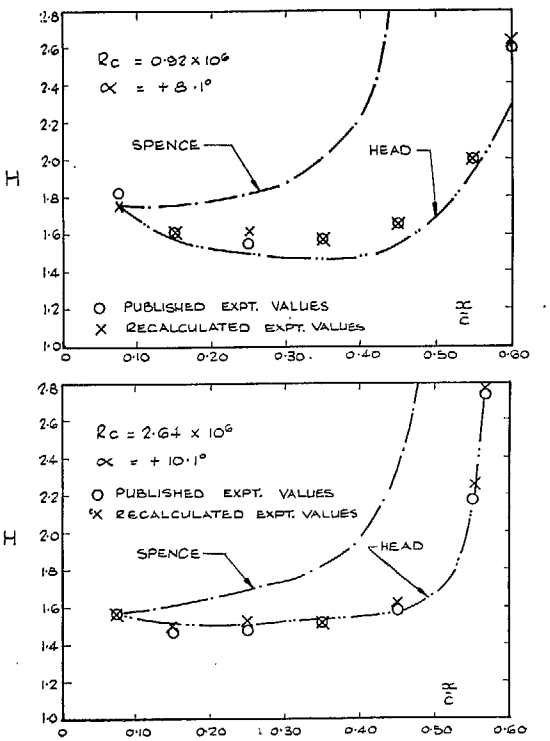

FIG. 22. von Doenhoff and Tetervin (13). [N.A.C.A. 65 (212)–222 aerofoil].

Comparison of calculated shape-factor developments.

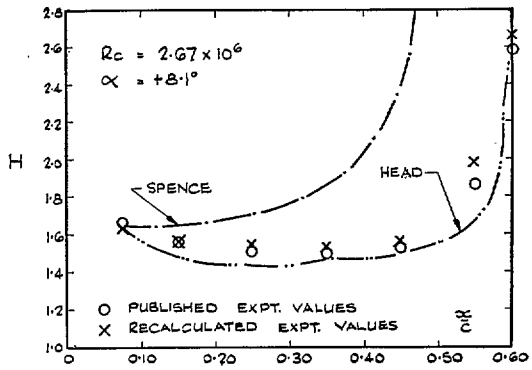

FIG. 23. von Doenhoff and Tetervin (13).
[N.A.C.A. 65 (212)–222 aerofoil].

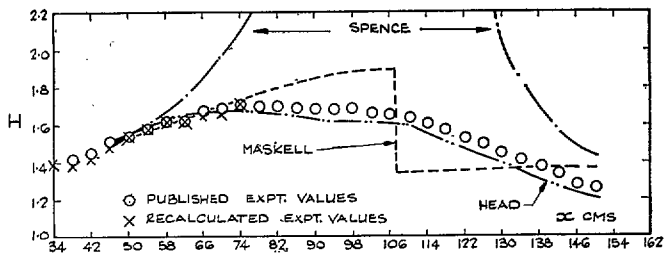

FIG. 24. Schmidbauer (52).

Comparison of calculated shape-factor developments.

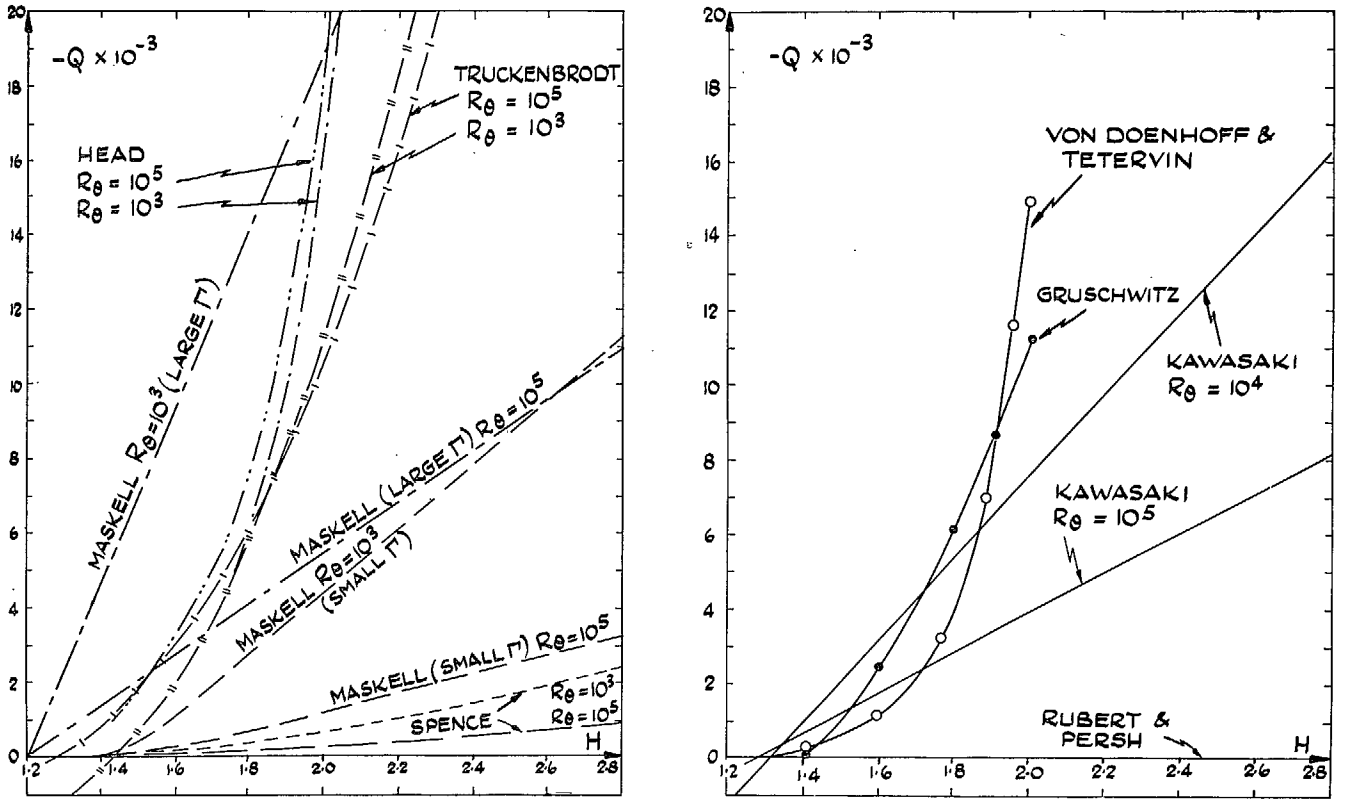

(a) Equations used in calculations.

(b) Equations not used in calculations.

FIG. 25. Comparison of auxiliary equations in terms of the generalised form.

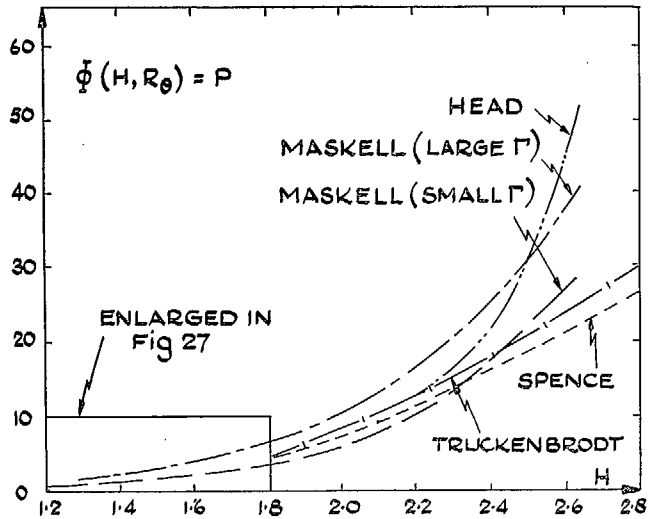

FIG. 26a. Equations used in calculations.

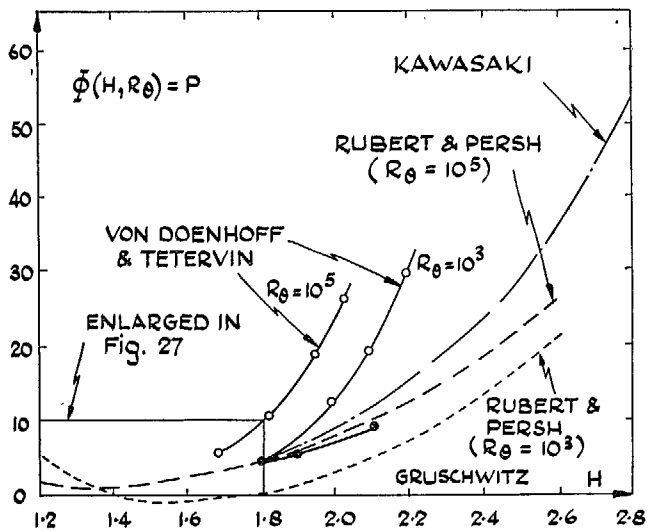

Fig. 26b. Equations not used in calculations.

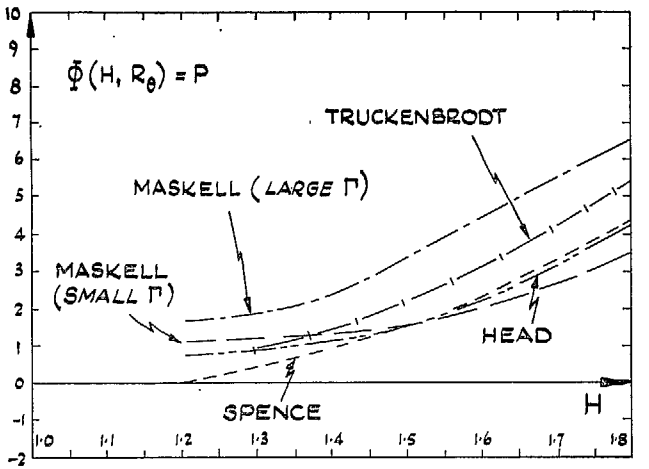

FIG. 27a. Equations used in calculations.

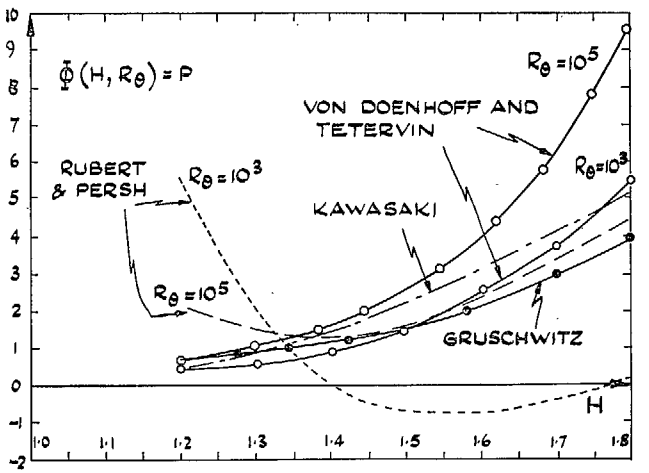

FIG. 27b. Equations not used in calculations.

Comparison of auxiliary equations in terms of the generalised form.

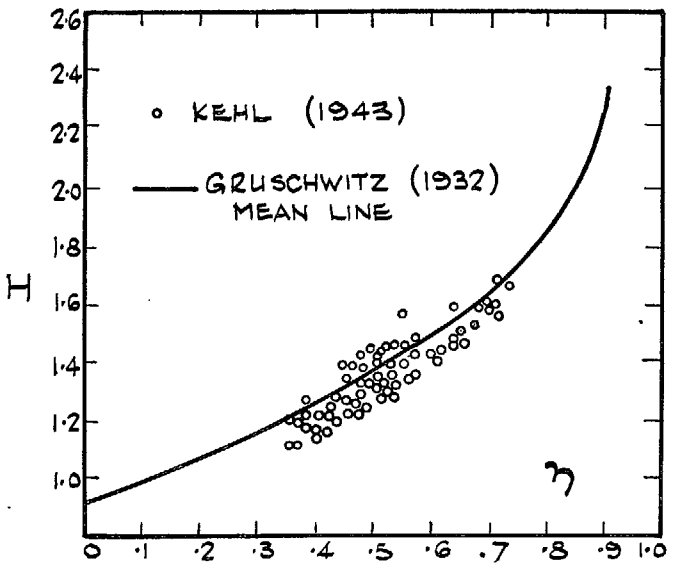

FIG. 28. Comparison of Gruschwitz shape-factor relationship with Kehl's experiments.

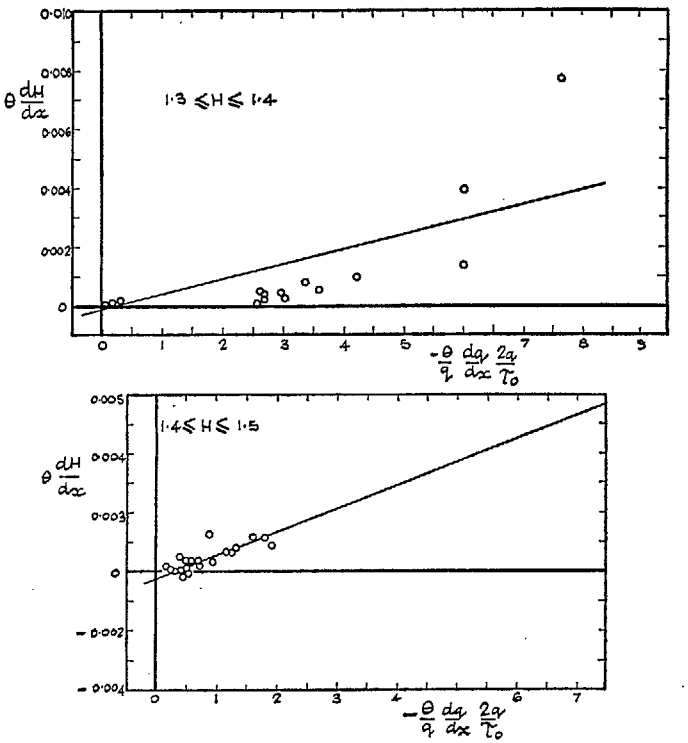

FIG. 29. Shape-factor correlation of von Doenhoff and Tetervin (13).

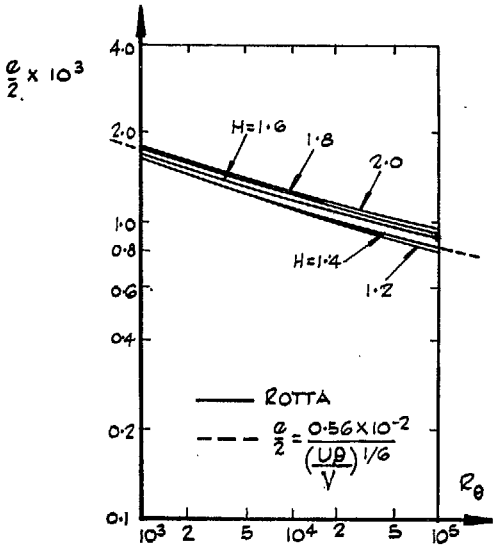

FIG. 30. Dissipation integral. Rotta. (45).

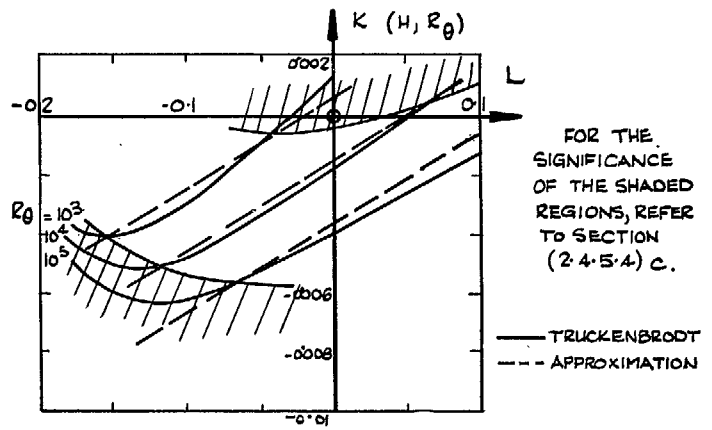

FIG. 31. Linear approximation to $K(L, R_\theta)$, [Truckenbrodt (71)].

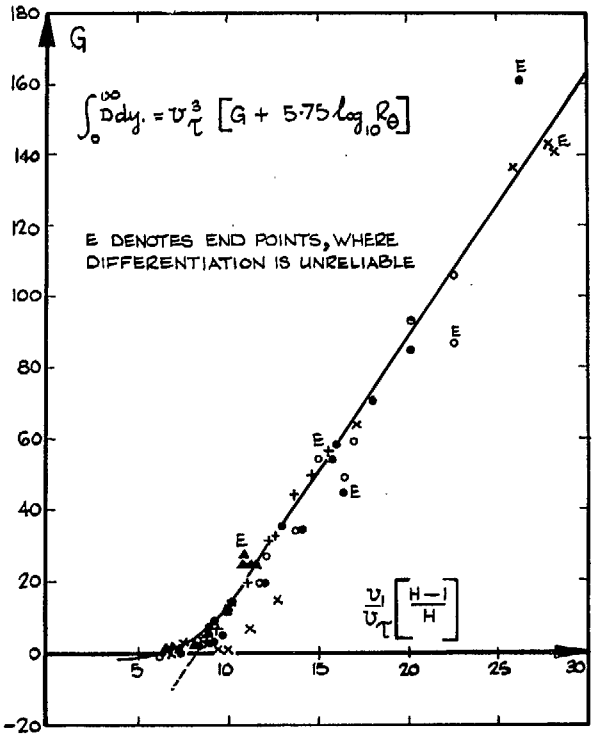

FIG. 32. Correlation for dissipation integral Rotta (45).

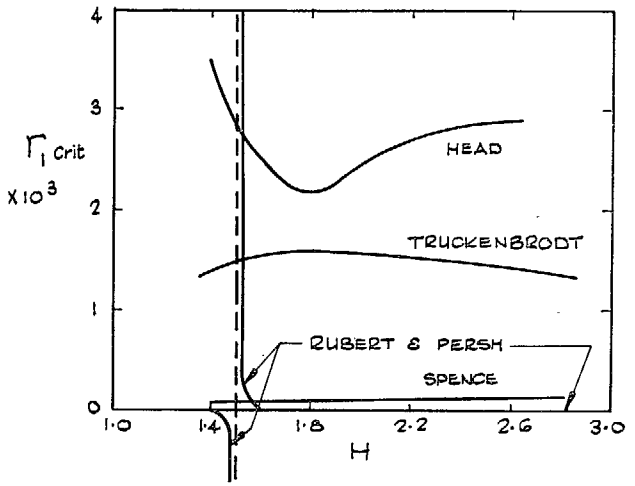

FIG. 33.

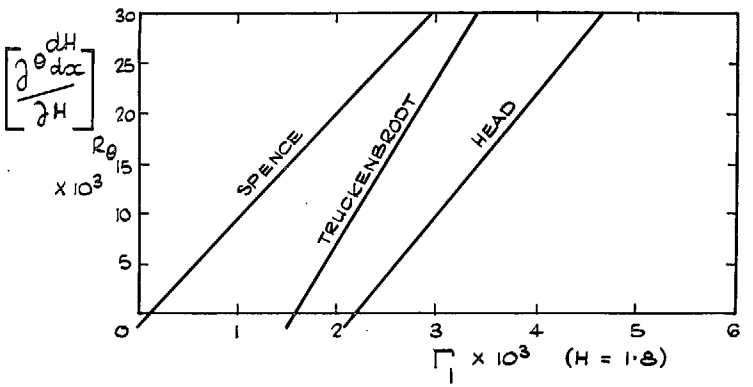

FIG. 34.

The stability characteristics of some typical auxiliary equations at $R_\theta = 10^4$.

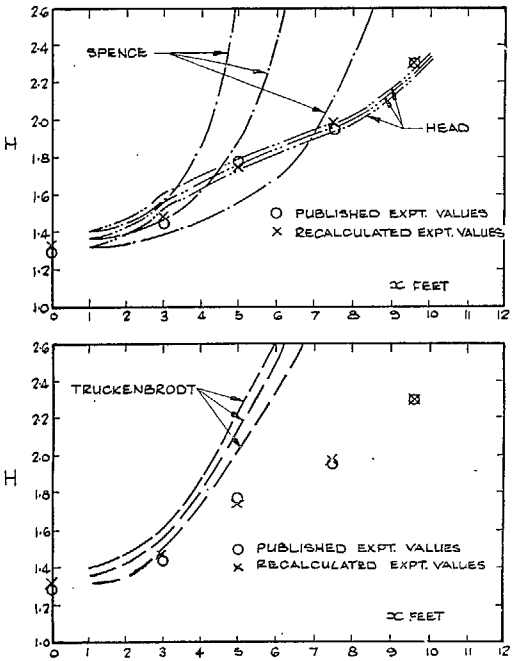

Schubauer and Spangenberg 'D' (54).

FIG. 35. The effect of initial values on calculated shape-factor development.

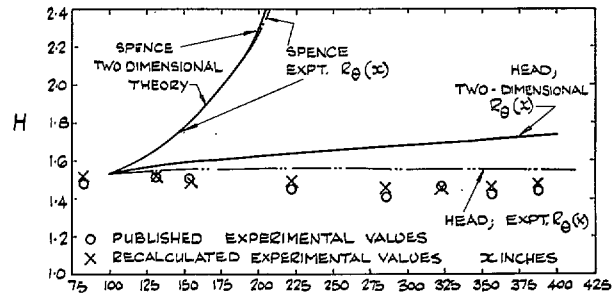

FIG. 36. Clauser (6) Series I.

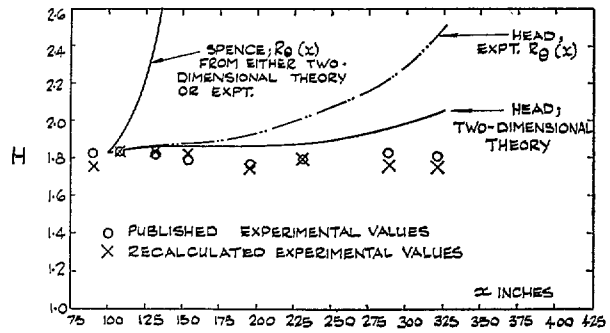

FIG. 37. Clauser (6) Series II.

The effect of assumed momentum growth on calculated shape-factor development.

(94656) Dd. 125874 K.5 2/67 Hw.

Publications of the Aeronautical Research Council

ANNUAL TECHNICAL REPORTS OF THE AERONAUTICAL RESEARCH COUNCIL (BOUND VOLUMES)

1945 Vol. I. Aero and Hydrodynamics, Aerofoils. £6 10s. (£6 14s.)
Vol. II. Aircraft, Airscrews, Controls. £6 10s. (£6 14s.)
Vol. III. Flutter and Vibration, Instruments, Miscellaneous, Parachutes, Plates and Panels, Propulsion. £6 10s. (£6 14s.)
Vol. IV. Stability, Structures, Wind Tunnels, Wind Tunnel Technique. £6 10s. (£6 14s.)

1946 Vol. I. Accidents, Aerodynamics, Aerofoils and Hydrofoils. £8 8s. (£8 12s. 6d.)
Vol. II. Airscrews, Cabin Cooling, Chemical Hazards, Controls, Flames, Flutter, Helicopters, Instruments and Instrumentation, Interference, Jets, Miscellaneous, Parachutes. £8 8s. (£8 12s.)
Vol. III. Performance, Propulsion, Seaplanes, Stability, Structures, Wind Tunnels. £8 8s. (£8 12s.)

1947 Vol. I. Aerodynamics, Aerofoils, Aircraft. £8 8s. (£8 12s. 6d.)
Vol. II. Airscrews and Rotors, Controls, Flutter, Materials, Miscellaneous, Parachutes, Propulsion, Seaplanes, Stability, Structures, Take-off and Landing. £8 8s. (£8 12s. 6d.)

1948 Vol. I. Aerodynamics, Aerofoils, Aircraft, Airscrews, Controls, Flutter and Vibration, Helicopters, Instruments, Propulsion, Seaplane, Stability, Structures, Wind Tunnels. £6 10s. (£6 14s.)
Vol. II. Aerodynamics, Aerofoils, Aircraft, Airscrews, Controls, Flutter and Vibration, Helicopters, Instruments, Propulsion, Seaplane, Stability, Structures, Wind Tunnels. £5 10s. (£5 14s.)

1949 Vol. I. Aerodynamics, Aerofoils. £5 10s. (£5 14s.)
Vol. II. Aircraft, Controls, Flutter and Vibration, Helicopters, Instruments, Materials, Seaplanes, Structures, Wind Tunnels. £5 10s. (£5 13s. 6d.)

1950 Vol. I. Aerodynamics, Aerofoils, Aircraft. £5 12s. 6d. (£5 16s. 6d.)
Vol. II. Apparatus, Flutter and Vibration, Meteorology, Panels, Performance, Rotorcraft, Seaplanes. £4 (£4 3s. 6d.)
Vol. III. Stability and Control, Structures, Thermodynamics, Visual Aids, Wind Tunnels. £4 (£4 3s. 6d.)

1951 Vol. I. Aerodynamics, Aerofoils. £6 10s. (£6 14s.)
Vol. II. Compressors and Turbines, Flutter, Instruments, Mathematics, Ropes, Rotorcraft, Stability and Control, Structures, Wind Tunnels. £5 10s. (£5 14s.)

1952 Vol. I. Aerodynamics, Aerofoils. £8 8s. (£8 12s.)
Vol. II. Aircraft, Bodies, Compressors, Controls, Equipment, Flutter and Oscillation, Rotorcraft, Seaplanes, Structures. £5 10s. (£5 13s. 6d.)

1953 Vol. I. Aerodynamics, Aerofoils and Wings, Aircraft, Compressors and Turbines, Controls. £6 (£6 4s.)
Vol. II. Flutter and Oscillation, Gusts, Helicopters, Performance, Seaplanes, Stability, Structures, Thermodynamics, Turbulence. £5 5s. (£5 9s.)

1954 Aero and Hydrodynamics, Aerofoils, Arrester gear, Compressors and Turbines, Flutter, Materials, Performance, Rotorcraft, Stability and Control, Structures. £7 7s. (£7 11s.)

Special Volumes

Vol. I. Aero and Hydrodynamics, Aerofoils, Controls, Flutter, Kites, Parachutes, Performance, Propulsion, Stability. £6 6s. (£6 9s. 6d.)
Vol. II. Aero and Hydrodynamics, Aerofoils, Airscrews, Controls, Flutter, Materials, Miscellaneous, Parachutes, Propulsion, Stability, Structures. £7 7s. (£7 10s. 6d.)
Vol. III. Aero and Hydrodynamics, Aerofoils, Airscrews, Controls, Flutter, Kites, Miscellaneous, Parachutes, Propulsion, Seaplanes, Stability, Structures, Test Equipment. £9 9s. (£9 13s. 6d.)

Reviews of the Aeronautical Research Council

1949–54 5s. (5s. 6d.)

Index to all Reports and Memoranda published in the Annual Technical Reports

1909–1947 R. & M. 2600 (out of print)

Indexes to the Reports and Memoranda of the Aeronautical Research Council

Between Nos. 2451–2549: R. & M. No. 2550 2s. 6d. (2s. 9d.); Between Nos. 2651–2749: R. & M. No. 2750 2s. 6d. (2s. 9d.); Between Nos. 2751–2849: R. & M. No. 2850 2s. 6d. (2s. 9d.); Between Nos. 2851–2949: R. & M. No. 2950 3s. (3s. 3d.); Between Nos. 2951–3049: R. & M. No. 3050 3s. 6d. (3s. 9d.); Between Nos. 3051–3149: R. & M. No. 3150 3s. 6d. (3s. 9d.); Between Nos. 3151–3249: R. & M. No. 3250 3s. 6d. (3s. 9d.); Between Nos. 3251–3349: R. & M. No. 3350 3s. 6d. (3s. 11d.)

Prices in brackets include postage

Printed and published by
HER MAJESTY'S STATIONERY OFFICE

To be purchased from
49 High Holborn, London W.C.1
423 Oxford Street, London W.1
13A Castle Street, Edinburgh 2
109 St. Mary Street, Cardiff
Brazennose Street, Manchester 2
50 Fairfax Street, Bristol 1
35 Smallbrook, Ringway, Birmingham 5
80 Chichester Street, Belfast 1
or through any bookseller

Printed in England

S.O. Code No. 23-3447